

ARAGONITE–CALCITE SPELEOTHEMS: IDENTIFYING ORIGINAL AND DIAGENETIC FEATURES

CHRISTINE PERRIN,^{1,2} LAURENT PRESTIMONACO,³ GUILHEM SERVELLE,⁴ ROMAIN TILHAC,⁴ MARION MAURY,⁴ AND PATRICK CABROL⁵

¹Station d'Ecologie Expérimentale à Moulis, USR 2936 du CNRS, 2 Route du CNRS, 09200 Moulis, France

²Centre de Recherches sur la Paléobiodiversité et les Paléoenvironnements, UMR 7207 du CNRS, Muséum National d'Histoire Naturelle, CP38, 8 rue Buffon, 75005 Paris, France

³Aquila Conseil, Parc Industriel de la Piche, Avenue Pierre Semard, 31600 Seysses, France

⁴LMTG, Université de Toulouse, 14 Avenue E. Belin, 31400 Toulouse, France

⁵DREAL Midi-Pyrénées, 1 rue Delpèch, 31000 Toulouse, France

e-mail: cperrin@mnhn.fr

ABSTRACT: Despite the increasing use of speleothems as high-resolution archives of past climate proxies, few efforts have been made to improve understanding of diagenetic pathways affecting this material and to assess the degree of postdepositional transformation of initial features, including associated geochemical signatures. To provide criteria for distinguishing primary (spelean growth history) and secondary (spelean diagenetic history) features, this study documents a process-based approach combining mineralogical, textural, and geochemical data at different scales to characterize various diagenetic processes undergone by aragonite and calcite speleothems from the Pont-de-Ratz Cave (Hérault, S. France). Results show that the initial precipitation of carbonate minerals forming the stalagmites (vadose precipitation) is represented alternatively by aragonite and calcite and consists of two types of primary aragonite and a primary columnar calcite. Four different types of growth interruption and inclusion horizons are evident, and attest to the discontinuous growth of stalagmites in this cave. Postdepositional diagenetic processes include void-filling calcite cementation, selective dissolution of either aragonite or calcite, and recrystallization. Recrystallization processes include 1) textural change of original aragonite precipitates (isomineralogical recrystallization), and 2) two distinct types of aragonite-to-calcite recrystallization. These results highlight the diversity of potential synformational and postformational processes controlling the formation and evolution of speleothems and their impact on the geochemical properties of the primary and secondary carbonate phases, and the potential importance in paleoclimatic interpretation.

INTRODUCTION

Over the past two decades, calcium carbonate speleothems have been used as an increasingly powerful terrestrial proxy, offering high-resolution records comparable to ice cores and varved lakes for the record of paleoclimate history for at least 600,000 years (e.g., Lauritzen and Lundberg 1999; Finch et al. 2001; Finch et al. 2003; McMillan et al. 2005; Soubiès et al. 2005; Tan et al. 2006; Asmeron et al. 2007; Lachniet 2009), with the potential to extend this record beyond one million years (Meyer et al. 2011). Their growth is linked via complex relationships to several climatic parameters such as temperature, rainfall amount and provenance, and humidity, making them excellent candidates as highly sensitive natural archives of climate changes (e.g., Fairchild et al. 2006a, 2006b; Ford and Williams 2007; Cheng et al. 2009; Drysdale et al. 2009; Asmeron et al. 2010; Onac and Forti 2011; Fairchild and Baker 2012). Their primary features (texture, mineralogy, geochemical composition) are strongly dependent from environmental parameters and, in particular: 1) the local microenvironment within the cave, 2) the geological and hydrogeological setting, and 3) the regional climatic conditions.

Some of these parameters change with time, yielding modifications of the physical and chemical microenvironment, which, in turn may result in postdepositional (diagenetic) alteration of the initial properties of the

speleothem. With evolving physicochemical conditions, the crystalline phases forming stalagmites and flowstones, the most common cave deposits used in paleoclimate studies, may become unstable. As a result, although these features potentially record the physicochemical conditions prevailing at the time of primary mineral precipitation, they also may reflect subsequent changes of these conditions during cave history. Such changes have been documented by the rapid diagenetic changes occurring in abiotic cave pearls over timescale as short as a few months (Melim and Spilde 2011), although the occurrence of biogenic processes in some other cave pearls (Jones 2009) can make those more prone to diagenetic modifications.

With the exception of few precursors (e.g., Thrailkill 1968; Fischbeck and Müller 1971; Folk and Assereto 1976; Cabrol 1978; Frisia 1996), most classical work on nonburial carbonate diagenesis, together with the understanding of related processes driving diagenetic modifications, has focussed on the marine realm (e.g., Purdy 1968; Bathurst 1971; Ginsburg et al. 1971; Aissaoui et al. 1986; Harris et al. 1985; Macintyre 1977; Schneidermann and Harris 1985; Morse et al. 2007; Perrin 2010). This is also the case for research concerning diagenetic evolution of carbonate cements and recrystallization of biogenic and abiogenic carbonate minerals (James 1974; Pingitore 1976; Gvirtzman and Friedman 1977; Mazzullo 1980; Sandberg 1984; Aissaoui 1985, 1988; Dullo 1986; Hover

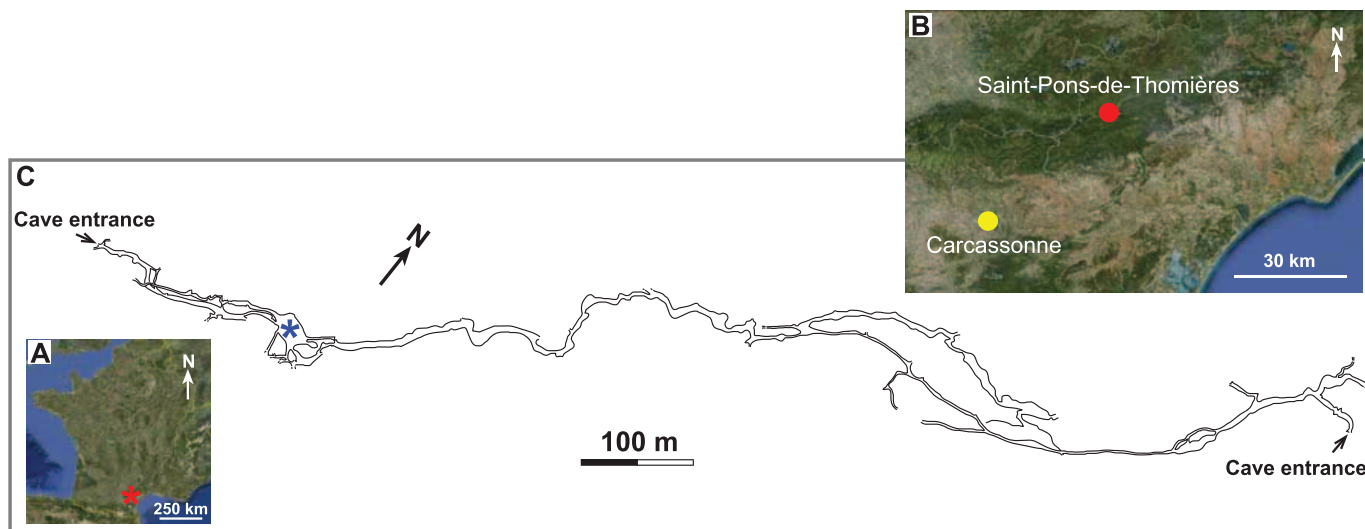


FIG. 1.—Location of the Pont-de-Ratz Cave and sampling site. **A)** General view indicating the location of the Pont-de-Ratz Cave (red star). **B)** Regional view indicating location of the cities of Carcassonne (yellow dot) and Saint-Pons-de-Thomières (red dot). **C)** Simplified plan-view map of the cave indicating the sampling site (blue star).

et al. 2001; Macintyre and Reid 1995, 1998; Perrin and Cuif 2001; Perrin 2004). Abiotic laboratory experiments on the physicochemical behavior of carbonate minerals provide the theoretical framework for inferring the links between petrographical and geochemical features, the nature and composition of diagenetic fluids, and the mechanisms involved in diagenetic processes (e.g., Badiozamani et al. 1977; Pingitore 1978, 1982; Buhmann and Dreybrodt 1985a, 1985b; Dreybrodt et al. 1996, 1997; Fernandez-Diaz et al. 1996; Pokrovsky et al. 2005; Perdikouri et al. 2008; Choudens-Sánchez and González 2009).

Diagenesis may cause alteration of geochronological and geochemical signal in speleothems and implications for U-series dating have been analyzed and discussed by Railsback et al. (2002), who considered petrography as a valuable tool for evaluating the suitability of speleothems for the extraction of geochronological information. Although several authors have emphasized the need for petrographic and chemical studies focused on the detection of diagenetic modifications of speleothems and assessment of factors controlling diagenetic pathways (Frisia et al. 2000; Fairchild et al. 2006a, 2006b; Fairchild and Baker 2012), few studies have actually targeted speleothem diagenesis (Cabrol 1978; Cabrol and Coudray 1982; Frisia 1996; Frisia et al. 2002; Railsback et al. 2002; Hopley et al. 2009; Martin-Garcia et al. 2009; Melim and Spilde 2011; Martin-Perez et al. 2012).

The aims of this work are to identify the diagenetic processes in aragonite and calcite speleothems from the Pont-de-Ratz Cave (Hérault, S. France) that impacted the deposits after initial precipitation of carbonate mineral, and to provide discriminant criteria for distinguishing primary (initial precipitation) and secondary (altered) features. Beyond the understanding of diagenesis in cave settings and postdepositional transformation of carbonate speleothems, an important objective of this work is to provide practical keys for the recognition of altered zones and for the selection of preserved primary spelean material for further more specific studies including paleoenvironmental research.

GEOLOGICAL AND HYDROLOGICAL SETTING

The Pont-de-Ratz Cave is located on the southern margin of the Montagne Noire, immediately south of the small city of Saint-Pons-de-Thomières (Hérault, S. France, Fig. 1). Geologically, this site is part of the allochthonous Saint-Ponais units of the southern Montagne Noire,

located between the axial zone to the north and the overthrust–nappe of Pardailhan to the south and composed of Ordovician to Devonian strata (Alabouvette et al. 1993).

The cave itself is cut into well-bedded Lower Devonian (Pragian–Lower Emsian) dolomite and limestone. It consists of three upper fossil levels and one lower active level where a small underground river flows to the NW, following the general orientation of the geological structures. The room where speleothems have been sampled for this study corresponds to a widening of the gallery in a river meander. At that site, a thick stalagmitic flowstone developed upon fluvial clastic deposits which consist mainly of schist pebbles and shales.

The present-day climate of the Saint-Pons area is influenced by both Mediterranean (SE) and Atlantic (W) air masses. These two main influences combined with the effect of relief exert strong controls on the spatial distribution of precipitation, with mean annual local record varying between 800 to 1500 mm. Precipitation and temperature data (Fig. 2) over the last 20 years (1993–2012) at the nearest meteorological station of Carcassonne (about 45 km SW of the Pont-de-Ratz Cave) record numerous changes. Monthly means indicate that precipitation maxima occur in spring and at the end of autumn, whereas precipitation minima are correlated with temperature maxima in July and August. Mean annual distribution of precipitation over the last 20 years shows a relatively drier period between 1993 and 1998, followed by a more humid period between 1999 and 2012 (Fig. 2).

METHODS AND MATERIAL

Twenty-two vadose speleothems, including stalagmites, stalactites, and stalagmitic flowstones, were collected in the same chamber of the Pont-de-Ratz Cave (Fig. 1). Fifteen specimens, including 13 stalagmites and two stalactites, were cut parallel to their vertical growth direction with a diamond saw to obtain two slabs from their middle. Each slab was cleaned and scanned, before observations at macroscopical scale and with a reflected-light binocular microscope.

Portable X-ray fluorescence (P-XRF) analyses were performed on slab surfaces of the speleothems using a portable energy-dispersive X-ray spectrometer (EDS) operating at 10–30 kV for a time analysis of ~ 60 seconds per point. Although the spatial resolution of this technique is relatively low (~ 1 cm-square for a sampling depth of a few

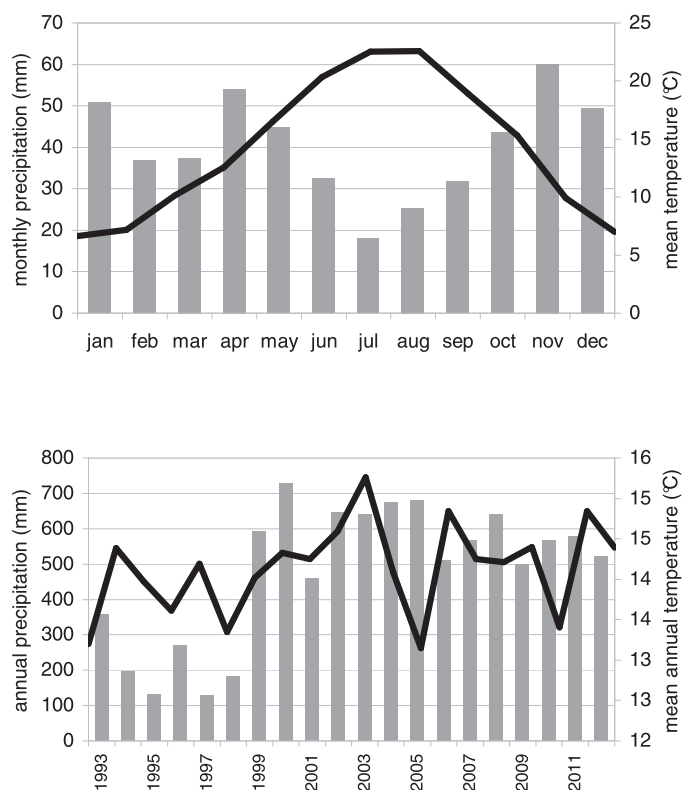


FIG. 2.—Precipitation and temperature records over 20 years (1993–2012) at the Carcassonne meteorological station. **A)** Monthly precipitation (gray bars) and mean temperature (black line) averaged for the last twenty years. **B)** Variability of annual precipitation (gray plots) and mean annual temperature (black line) over the last twenty years.

micrometers), the detection threshold for most trace elements commonly found in carbonate speleothems remains lower or about the same than with the wavelength-dispersive X-ray spectrometry (WDS) microprobe. This P-XRF technique, however, does not allow Mg to be detected. In these samples, limits of detection are: 180 ppm (Mn), 180 ppm (Fe), 30 ppm (Zn), 4 ppm (Sr), and 30 ppm (Zr).

For each speleothem, one slab was kept as a reference while the other was thin-sectioned and subsampled for scanning-electron-microscopy (SEM) and microprobe preparations. Twenty-eight large thin sections (6 cm × 4 cm in size and 20–25 µm in thickness) were cut parallel to the axial growth direction of the stalagmites and stalactites, and prepared for conventional optical petrography studies. A second set of subsamples was cut using a dental diamond micro-saw, cleaned in an ultrasonic generator, and prepared for SEM and microprobe analyses. Scanning electron microscopy was performed on either freshly broken surfaces or on polished surfaces obtained by using successive finer-grained carborundum and, finally, diamond paste. In addition, some polished samples were slightly etched for 20–30 seconds in acetic acid 1% weight, then rinsed in demineralized water and air dried, similarly to method previously described (e.g., Perrin 2003). All SEM samples were carbon-coated. Observations and qualitative elementary analyses were made using a JEOL JSM 6360 LV working between 10 and 20 kV and a TESCAN VEGA 2 LSU working at 15 kV. Both SEM microscopes are equipped with secondary-electron (SE) and backscattering-electron (BSE) detectors, and each is coupled to a SDD-EDS detector system allowing either qualitative (Sahara PGT, JEOL SEM) or semiquantitative (Type Bruker, TESCAN SEM) elementary micro-analyses to be performed.

SEM polished surfaces were examined for quantitative elementary analyses with an electronic WDS microprobe CAMECA SX50 working with an accelerating voltage of 15 kV and a beam current of 40 nA. The Mg, Ca, Mn, Fe, Sr, and Ba contents of the different carbonate minerals were obtained with a spatial resolution of 10–40 µm and detection limits of: 200 ppm (Mg), 300 ppm (Ca), 350 ppm (Mn), 450 ppm (Fe), 450 ppm (Sr), and 650 ppm (Ba).

First documented by Raman and Krishnan (1928), the Raman effect is an inelastic molecular scattering process resulting from interaction between matter and light. Designed in the 1970s (Delhay and Dhamelincourt 1975; Dhamelincourt and Bisson 1977), Raman microspectrometry provides information about the high-spatial-resolution molecular environment of asymmetrically and symmetrically vibrating bonds, and hence has long been used for nondestructive physicochemical analysis of various materials, including minerals (see Nasdala et al. 2004, for a review about applications in mineralogy). In the context of this speleothem study, Raman microspectrometry is used for obtaining complementary mineralogical identifications. Selected polished samples, including some SEM samples which have been slightly polished again to remove the carbon coating, were analyzed with a Jobin Yvon Horiba HR800 LabRam® spectrometer operating with a green 514.5 nm exciting line using ~ 10 mW on sample, and with a 1 µm spatial filter (a pseudo-confocal system to reduce analysis at depth). Before each analysis session, the potential deviation of the microspectrometer measurements was checked by measuring the spectrum of a quartz crystal, and corrected if needed. Analyses were performed with a spectral window of 130–1600 cm⁻¹. This technique allows qualitative analyses to be performed with a spatial resolution of about 1–2 micrometers. The system is associated with an optical microscope in reflected light and a video camera, allowing the analytical spot to be precisely positioned.

ANALYTICAL APPROACH AND TERMINOLOGY

The general analytical approach used in this study is the process-based approach classically used by carbonate sedimentologists and petrographers in carbonate diagenetic research. This approach relies strongly on the detailed petrographical analysis of thin sections under the optical microscope from which the various diagenetic products and their spatial, and chronological, relationships are characterized. Complementary geochemical, ultrastructural, and mineralogical data are provided for each product by using a step-by-step suite of analytical methodologies. The latter are used successively for the analysis of particular features, depending on questions arising from the results obtained from the preceding analytical step.

Finally, petrographical relationships between various crystalline phases, their relationships with introduced other phases (such as clay, particulate, and colloidal organic matter), as well as with diagenetic modification events affecting previous carbonate phases through dissolution or recrystallization, allow the paragenetic sequence to be constructed. This, combined with the spatial distribution of the various identified products at the scale of stalagmite specimen, whose growth direction is oriented from its base to its external surface, leads to establishment, step by step, of a relative chronology of stalagmite growth processes and diagenetic history. For these reasons, the regularity of stalagmite growth, which results in a broad predictable internal architecture, with time gradients oriented from base to top and from its internal part to its external surface, offers a more highly promising potential than stalactites.

This study makes a distinction between the morphology or habit of individual crystals (i.e., crystal shape and size), and the fabric or texture, which depicts the spatial arrangement of individual crystals within a set of crystals (for example the fan-shape arrangement of fibrous crystals) and the geometric relationships between sets of crystals. The morphology or

habit of a crystal is determined by the crystal structure, the crystal growth conditions, and the process of that growth, whereas the fabric or texture results from the interaction between crystals during the growth process, in particular the time and density of nucleation, the morphologies of single crystals, and the competitive growth in crystal aggregates (Dickson 1983, 1993; Self and Hill 2003; Sunagawa 2005).

The terms “primary” aragonite and “primary” calcite refer to direct precipitation of carbonate minerals on the external surface of a speleothem from a supersaturated solution (drip water), and therefore to the major process leading to the growth of speleothems. “Cement” is used to describe precipitates within primary or secondary pores of an already formed speleothem. The latter void-filling cements are in most cases phreatic or microphreatic, but we describe in this paper discrete cements developed in stalagmite porosity in a vadose setting.

Herein, the term recrystallization is used in its general sense: a reorganization of the size, shape, texture and/or composition of original crystals without major mineralogical changes, following the definition of Sorby (1882 in Folk 1965) and Purdy (1968). We used this term to describe transformation of a precursor into either the same mineral or a polymorph, as have several previous workers (e.g., Machel 1997; Reid and Macintyre 1998; Railsback et al. 2002; Perrin 2004; Melim and Spilde 2011), and therefore include in this definition the neomorphism (i.e., transformation of a mineral into a polymorph) of Folk (1965). Some authors, such as Frisia et al. (2002), have used the term replacement, with a similar meaning, but this study restricts the term to its strict sense, for mineralogical transformation involving major compositional change (e.g., dolomitization) (Folk 1965).

The terms fibrous (i.e., with a length-width ratio of 6:1) and columnar are used to describe elongated crystal morphology (Kendall and Broughton 1978; Frisia and Borsato 2010). Acicular refers to material composed of elongated (typically with a minimum length-width ratio of 6:1) and pointed (i.e., needle-like) crystals that are less than 10 μm wide, independently of the mode of packing of these crystals. Ray is used to describe fibrous crystals having square terminations (Frisia and Borsato 2010). Columnar is used to describe crystals that are elongated but with a length-width ratio less than or up to 6:1 (Frisia and Borsato 2010). Typically, columnar crystals are wider than 10 μm . We use more specifically the term bladed to describe crystals that are not equidimensional and not fibrous, typically with a length-width ratio between 1.5:1 to 6:1 and with broad-flattened terminations (Flügel 2010).

RESULTS

Age of Samples

Following the diagenetic study presented here, parts of stalagmites not affected by postdepositional diagenesis and composed exclusively of primary aragonite or primary calcite have been carefully selected and sampled for U/Th dating. Although detailed dating of the speleothem samples for establishing a full geochronology of events is beyond the scope of this paper and will be published elsewhere, the oldest U/Th age found in the samples presented here is of 8244 ± 141 years, indicating that all the processes described below, including growth and diagenetic alteration of these speleothems, took place during the Holocene.

Identification of Minerals

Mineral species identified from their optical properties are evident with the petrographical microscope in transmitted light. Since distinction of calcite and aragonite is sometimes difficult under the optical microscope, especially in the case of small crystals, complementary identification was carried out by Raman microspectrometry of polished sections corresponding either to the same surface of thin sections or to samples

TABLE 1.—Assignment of Raman bands (cm^{-1}) detected in the speleothems of Pont-de-Ratz Cave.

Vibration Assignment	Aragonite	Aragonite & Calcite	Calcite
Lattice mode	142		
	180	154	
	206		
	213		
T(Ca, CO_3)	248		
	261		
	272		
T(Ca, CO_3)		282	
ν_4 symmetric CO_3 deformation	701		
	705		
	716		712
ν_2 asymmetric CO_3 deformation	853		
ν_1 symmetric CO_3 stretching		1085	
ν_3 asymmetric CO_3 stretching			1435
	1461		
	1573		

analyzed with SEM and microprobe. Sixty-six Raman spectra were measured on these samples.

Several bands in Raman spectra are common to both aragonite and calcite (Table 1). This is the case for the strong 1085 cm^{-1} band characterizing the ν_1 symmetric stretching vibration of CO_3 , although this band is observed at $1086\text{--}1087 \text{ cm}^{-1}$ in calcite. Other bands common to both polymorphs are the well-known 154 cm^{-1} band attributed to a lattice vibration, together with the 282 cm^{-1} typical of the T(Ca, CO_3) vibration mode. The two first bands were recorded in all spectra, whereas the third seems to be more dependent on the crystal orientation relative to the laser beam. We used the ν_4 symmetric CO_3 deformation bands in the $701\text{--}717 \text{ cm}^{-1}$ region, together with the ν_3 asymmetric CO_3 stretching bands of the $1434\text{--}1574 \text{ cm}^{-1}$ region for efficiently discriminating aragonite and calcite, similarly to Perrin and Smith (2007a, 2007b) for the coral skeletons. The ν_4 symmetric CO_3 vibration in the aragonite is recorded by a $701\text{--}705 \text{ cm}^{-1}$ doublet together with a 717 cm^{-1} weaker band, whereas the calcite in this region shows a single band at 712 cm^{-1} . The ν_3 asymmetric CO_3 stretching vibration is expressed by two strong bands at 1461 and 1573 cm^{-1} in aragonite and one weak band at 1435 cm^{-1} in calcite (Table 1).

Three different types of spectra (Fig. 3) include either one single mineral species (aragonite or calcite, Fig. 3A and B, respectively), or both occurring together (Fig. 3C). Most importantly, the detailed determination of Raman bands allows the mixture of both polymorphs at fine spatial scale (typically submicrometer scale) to be recognized even when only one mineral (generally calcite) evident with the optical microscope or the SEM, in particular in recrystallized zones (see below).

Primary Aragonite

Primary Acicular and Ray Aragonite.—In slab specimens, this type of primary aragonite presents a fibrous texture and a white, nearly opaque aspect, which is related to both the small width of crystals and to the relatively high microporosity of this crystal arrangement. Growth laminae can be distinguished clearly in some samples (Fig. 4A), whereas in others, laminae are not visible.

The *acicular aragonite* (Fig. 4) is composed of needle-like crystals elongated along their *c* axis, with a pointed termination. These crystals generally have a width-length ratio of 1:15 or less (a few micrometers

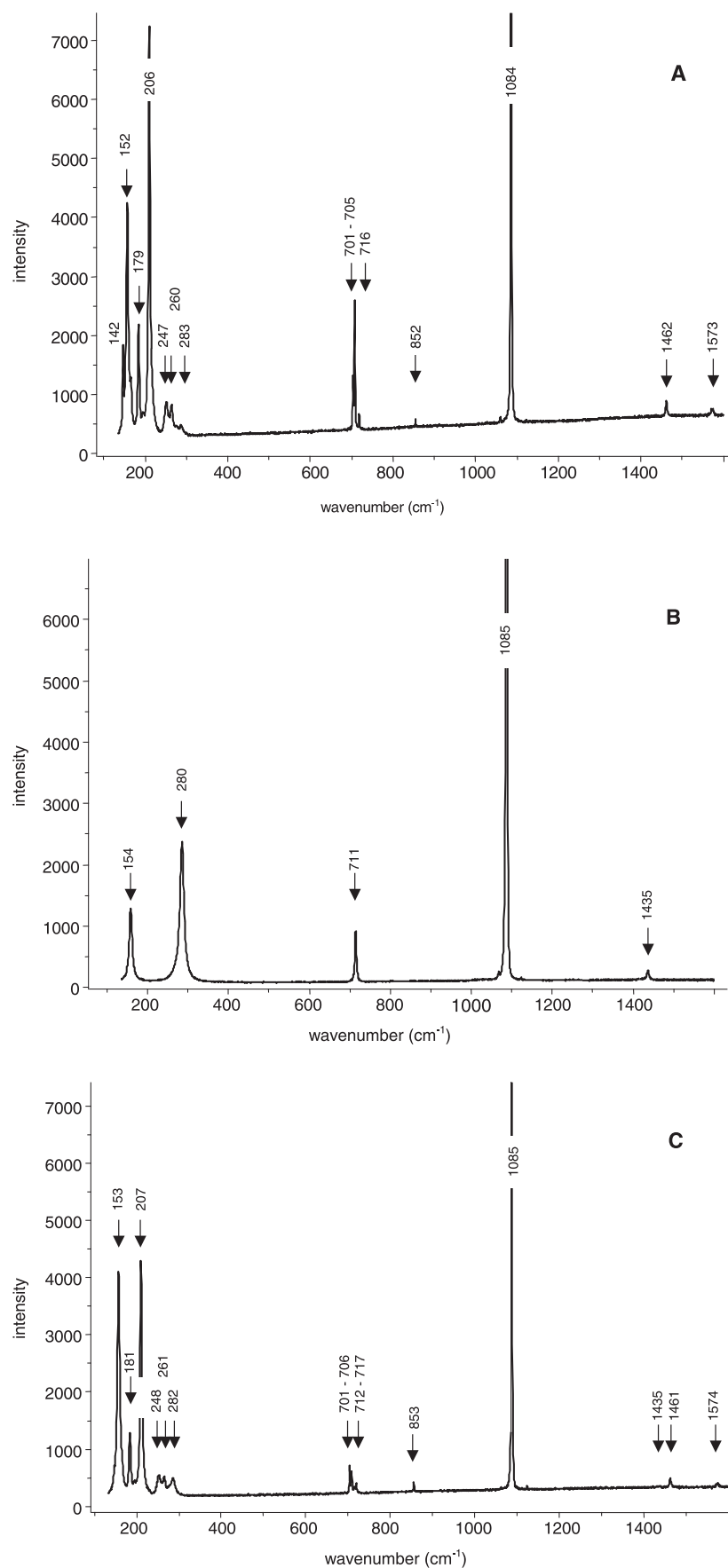


FIG. 3.—Three typical Raman spectra from Pont-de-Ratz Cave. **A)** Aragonite showing the typical vibrations of aragonite (see Table 1 for detail). **B)** Calcite characterized by the 711 and 1435 cm^{-1} bands. **C)** Aragonite and calcite are both identified: spectrum shows bands typical of aragonite (for example 701–706, 717, 1461, 1574 cm^{-1}) and bands typical of calcite (for example, 717 and 1435 cm^{-1}).

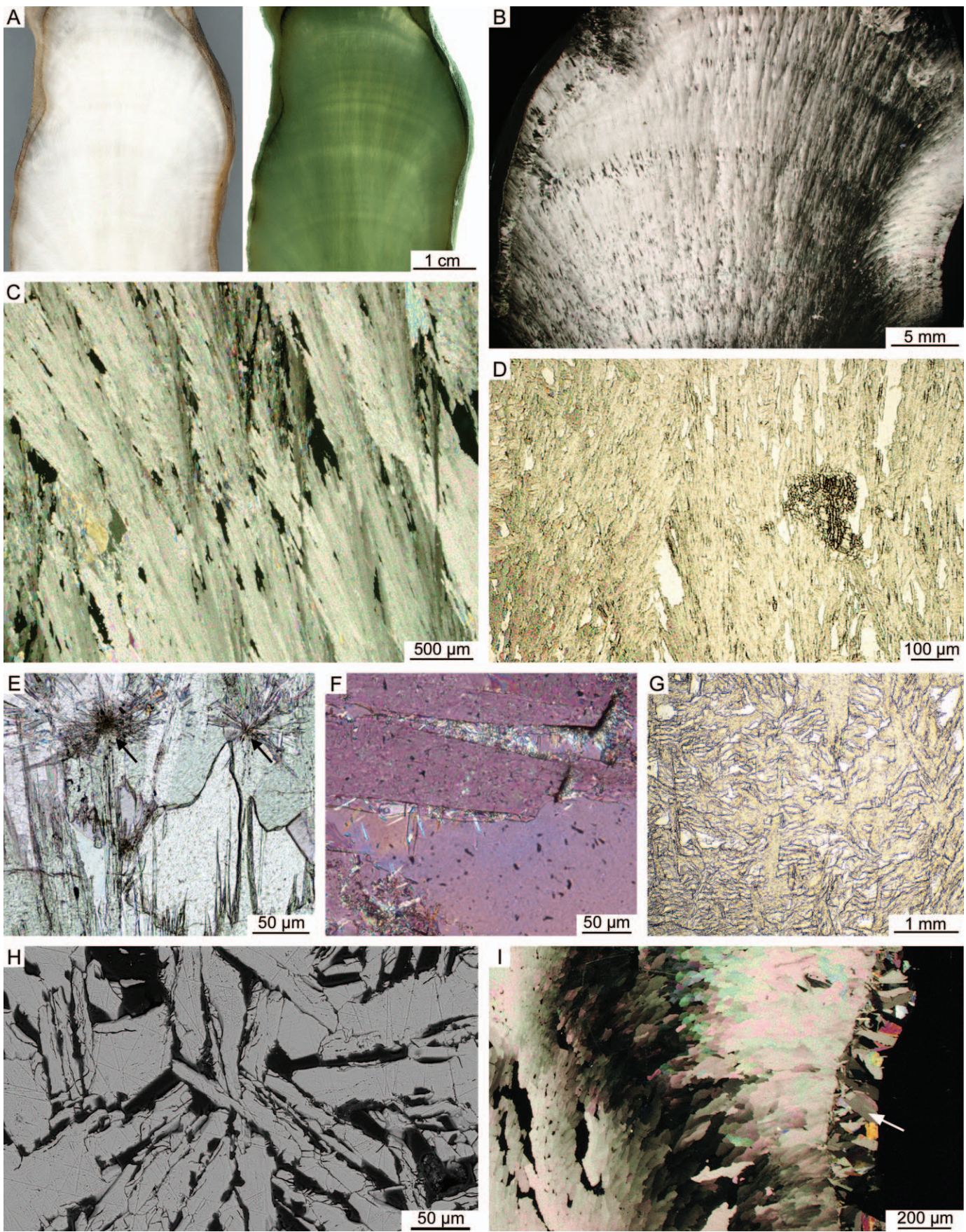


TABLE 2.—*Synthesis of WDS microprobe elemental analyses. N, number of analyses. Results below detection limit are indicated by a dash (see text “Methods and Material” for detailed values of limits of detection).*

Nature	N		Mg	Mn	Fe	Sr
Primary acicular and ray aragonites	11	Range (ppm)	-	-	-	570–1241
		Mean value (ppm)	-	-	-	821
		Standard deviation (ppm)	-	-	-	188
Primary ray aragonite (divergent crystal orientations)	16	Range (ppm)	-	-	-	542–1308
		Mean value (ppm)	-	-	-	829
		Standard deviation (ppm)	-	-	-	232
Primary bladed aragonite	13	Range (ppm)	-	-	-	550–1572
		Mean value (ppm)	-	-	-	1025
		Standard deviation (ppm)	-	-	-	235
Primary columnar calcite	19	Range (ppm)	3917–8649	-	-	-
		Mean value (ppm)	6588	-	-	-
		Standard deviation (ppm)	1268	-	-	-
Early cement of small isolated rhombohedrons	6	Range (ppm)	7018–9546	-	-	-
		Mean value (ppm)	8646	-	-	-
		Standard deviation (ppm)	1138	-	-	-
Recrystallization aragonite	2	Range (ppm)	-	-	-	756–1072
		Mean value (ppm)	-	-	-	914
		Standard deviation (ppm)	-	-	-	223
Recrystallization sparry calcite	8	Range (ppm)	up to 609	-	-	-
		Mean value (ppm)	107	-	-	-
		Standard deviation (ppm)	221	-	-	-
Recrystallization columnar calcite	11	Range (ppm)	5278–12483	-	-	-
		Mean value (ppm)	7848	-	-	-
		Standard deviation (ppm)	2426	-	-	-

width and 50–100 μm in length). Most commonly, these acicular crystals are packed densely together, typically forming narrow fans of radiating crystals, with apical openings of 20–30° and the median symmetry axes of fans perpendicular to the growth surface. Apices of fans occur upon nucleation surfaces, and the growth of individual radiating crystals produces the widening of individual fans which results in spatial competition between neighbouring fans. This arrangement directly controls the distribution of primary porosity: interfan primary porosity is higher above nucleation surfaces and tends to diminish gradually with the increasing widening of fans parallel to the growth direction (Fig. 4B–D). On slab surfaces, this feature forms growth laminae clearly observable at macroscopic scale (Fig. 4A).

Thin pointed needle-like crystals 1–2 μm wide for 10–15 up to 50–100 μm long are evident in some samples. The individual neighboring crystals commonly show markedly divergent *c* axes and can form open fan-spherulites (Fig. 4E). This micro-needle-like aragonite commonly occurs upon crystalline faces of larger crystals (Fig. 4F) or directly on top of a thin argillaceous layer. These needle crystals seem to nucleate and develop after a growth interruption of the stalagmite, either after the larger columnar crystals ceased to grow or after the deposit of clay. They represent an early growth stage of the primary acicular aragonite.

The primary ray aragonite consists of larger aragonite crystals, about 30–200 μm wide and several hundreds micrometers long, often with prismatic morphology. These ray crystals can have very different, and even divergent, orientations, this arrangement preserving much more primary intercrystalline porosity compared to the fan-like fabric (Fig. 4G, H). At first glance, zones composed of ray crystals with

divergent orientations mimic dendrites. However, dendritic crystals are characterized by branching morphologies, which are not evident in these samples. The gradual lateral change from the fan-like fabric of acicular aragonite to the divergent ray crystals is apparent in several thin sections.

WDS analyses show that this acicular aragonite has an Sr content varying from 570 to 1241 ppm (average 821 ppm), and no Mg was detected. The primary ray aragonite with divergent-crystal fabric has a similar elemental composition, with an average Sr content of 830 ppm (Table 2). XRF analyses on the stalagmite slabs yielded Sr content between 651 and 725 ppm (average 714 ppm) for the white fibrous zones corresponding to the acicular aragonite. In these areas, detectable concentrations of Mn (up to 367 ppm), Fe (up to 300 ppm), or Zr (up to 57 ppm, Table 3) are probably related to the presence of small amounts of clay between aragonite crystals.

Primary Bladed Aragonite.—On the polished slab surfaces, this aragonite forms a light-brown to yellow fringe, a few millimeters to less than one centimeter thick. It represents the uppermost carbonate layer in most stalagmites (Fig. 4I). It consists mainly of bladed aragonite crystals with tabular terminations. These crystals are typically 20–40 μm wide and 60–150 μm long, although some fine and elongated ray (10 μm across and 30–100 μm long) crystals also occur within the same layer. Individual neighboring crystals often show highly diverging orientations (Fig. 4I) or form asymmetric open fans. A consequence of this fabric is the high intercrystalline porosity of the layers composed of this type of aragonite. The Sr content of the bladed aragonite, as shown by the WDS analyses, ranges between 550 and 1572 ppm (average 1025 ppm) (Table 2).

←

FIG. 4.—Character of primary aragonite. **A)** Macroscopic view of acicular aragonite in reflected and transmitted light showing growth banding, part of stalagmite slab. **B, C)** Acicular aragonite showing a fan-like arrangement of fibrous crystals, interfan porosity, higher at the fan-apex level, produces the growth banding pattern; thin section, polarized light, crossed nicols. **D)** Closer view of crystal arrangement in two neighboring fan-like structures; thin section, polarized light. **E, F)** Needle-like aragonite; thin section. **E)** Two fan spherulites of aragonite needles (arrows) preserved in low-magnesium sparry calcite of recrystallization; polarized light. **F)** Aragonite needles developing on larger crystals; polarized light, crossed nicols. **G, H)** Primary ray aragonite crystals with divergent orientations. **G)** Thin section, polarized light. **H)** Morphology of individual crystals and microporosity (black areas) preserved between crystals. SEM. **I)** Bladed aragonite (white arrow) on columnar calcite; thin section, polarized light, crossed nicols.

TABLE 3.—*Synthesis of P-XRF spectrometry elemental analyses of primary carbonate phases. N: number of analyses. < LOD: results below detection limit (see text “Methods and Material” for detailed values of limits of detection).*

Nature	N		Mn	Fe	Zn	Sr	Zr
Primary aragonite	14	Range (ppm)	up to 367	up to 298	< LOD	651–725	up to 57
		Mean value (ppm)	85	74		714	
		Standard deviation (ppm)	137	115		42	not significant
Primary columnar calcite	68	Range (ppm)	up to 452	up to 3162	< LOD	50–93	
		Mean value (ppm)	49	636		70	< LOD
		Standard deviation (ppm)	126	660		10	

Primary Calcite

Primary Columnar Calcite.—In polished slab, this calcite appears translucent, either uniform gray or including lighter whitish irregular patchy areas (Fig. 5A). The lighter whitish zones are not distinguished in transmitted light with an optical microscope; their aspect appears to be related to the orientation of individual crystals that differs from the surrounding areas. Growth laminae can be visible clearly either directly on the slab surface (Fig. 5A) and in transmitted light. The stratigraphic position of this primary calcite varies depending on the stalagmite specimen considered, attesting to several phases of columnar calcite precipitation in the Pont-de-Ratz Cave.

The primary columnar calcite consists of elongated crystals about 150–200 μm wide and several millimeters and up to 20 millimeters long. Crystals typically have pointed terminations, and their faces, including the termination faces, are commonly curved. Under crossed polars, these crystals show sweeping extinction, particularly in curved crystals (Fig. 5B, C). The individual columnar crystals can coalesce, leading to a compact fabric with few primary intercrystalline pores. Crystals are oriented subparallel to the growth direction, commonly with an apparent increasing curvature of crystal sets towards the external margins of the stalagmite (Fig. 5C). Whereas the macroscopical aspect of this calcite can vary in color depending on the presence of clay particles, in the homogeneity of its translucent texture, and in the aspect of the growth lamination, its petrographical characteristics remain unchanged.

EDS and WDS microprobe analyses show that the average Mg content of the primary columnar calcite is ~ 5600 and ~ 6600 ppm respectively, whereas its Sr content is always below the limit of detection (Table 2). No significant differences are evident between the homogeneous translucent zones and the whitish irregular patches in X-ray fluorescence performed on slab surfaces. XRF results show that the Sr content of this columnar calcite varies between 50 and 93 ppm, averaging 70 ppm. The low Fe and Mn contents in the areas of primary columnar calcite are attributed to minor clay particles in the intercrystalline porosity (Table 3).

Calcite Cement

Sparite Cement.—This calcite cement is composed of equant crystals of highly variable size, generally several tens to a few hundreds of micrometers, and developed in primary intercrystalline voids (Fig. 5D, E) of an already existing spelean structure. In addition to the larger size of crystals forming the sparite cement relative to the small isolated rhombohedral crystals (described below), the main difference between these two cements and is that the sparite cement developed in porosity independent of the nucleation substrate, whereas the isolated rhombohedrons typically crystallize upon surfaces of ray aragonite crystals.

Isolated Rhombohedral Crystals.—This calcite cement is characterized by small rhombohedral crystals, 20 to 150 μm wide, which occur isolated or in small groups of several contiguous crystals. These calcite crystals

typically develop on the surfaces of ray aragonite crystals where intercrystalline porosity is relatively high. Isolated individual rhombohedral crystals display almost perfect crystalline shape, whereas contiguous crystals show common intercrystalline boundaries resulting from growth competition between neighboring crystals (Fig. 5F). Variability of this cement mainly concerns the size of crystals, but their shape and type of occurrence remain the same in the studied speleothems. They are commonly found in areas where recrystallization of large-sized aragonite crystals proceeds. EDS and WDS analyses indicate that these calcite crystals have an Mg content between 7000 and 10,000 ppm (Table 2).

Growth Surfaces, Discontinuities, and Inclusion Levels

Four different types of growth interruption surface and growth discontinuity are distinguished (Figs. 6–8). Each type includes some subtypes, which are described below, several of them being similar or comparable to the growth layering and inclusion patterns reported in the pioneering study of Kendall and Broughton (1978) and in subsequent work (e.g., Berthaux et al. 2002; Meyer et al. 2009; Railsback et al. 2011). Lateral passage from one type or subtype to another one is common.

Growth Surface Related to One or Several Inclusion Levels.—Inclusions of colloidal particles or aerosols are trapped within crystals by the advancing growing surface. As such, they present two important points in the understanding of speleothem growth history: first, they can influence growth in several ways and, hence, fabric of the subsequent crystals (see below); second, they likely represent the former external surface of the stalagmite.

Inclusion horizons include two different types in these samples. In all cases, inclusions are less than one micrometer in size, therefore preventing the nature of inclusions to be identified with certainty with the light microscope.

Type 1: The individual inclusions are distinct at high magnification. They are grouped in a horizon, within which the concentration of inclusions is sufficient to define a thin dark layer. Several successive parallel layers are common. These layers follow former positions of crystalline terminations, and hence correspond to a former external surface of the stalagmite (Fig. 6A, B). In some cases, inclusion layers are thin and discontinuous (Fig. 6C). The morphology of crystal terminations lined by the inclusion layer depends on the mineralogy of these crystals, whereas the height of crystalline terminations depends on the thickness of the water film from which they grew.

Type 2: Inclusions are too small to be distinguished individually at the optical microscope scale. These types form levels with a yellow to light brown color within the carbonate crystals, which can sometimes show small discrete micro-inclusions (Fig. 7A–C).

Growth Surface Marked by a Detrital Layer.—This type of discontinuity is represented by a thin detrital layer, composed mainly of clay and identified macroscopically at the scale of the stalagmite specimen and petrographically in thin section. Such discontinuities define former external growth surfaces of stalagmite (Fig. 6C, 8A, B). At the sample

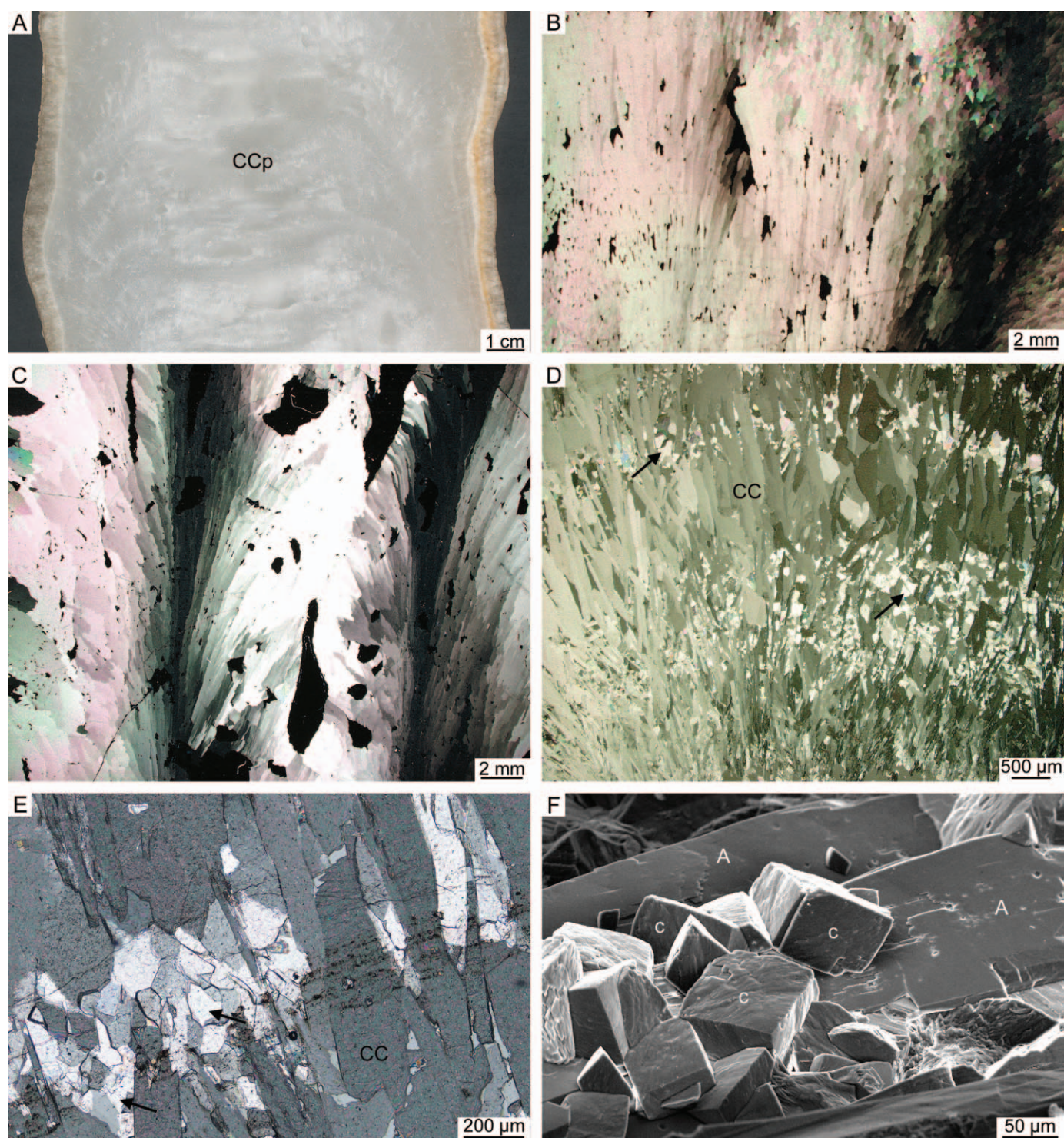


FIG. 5.—Primary calcite and calcite cement. A–D) Axial vertical growth direction of stalagmites is oriented toward the top of microphotographs. A) Macroscopic view of primary columnar calcite (CCp) in reflected light, part of stalagmite slab. B, C) Primary columnar calcite showing sweeping extinction and curved-face elongated crystals; thin section, polarized light, crossed nicols. D) Secondary sparry calcite cement (arrows) developed in residual primary porosity of columnar calcite (CC); note that this cement occurs at several stratigraphical “levels” relative to stalagmite axial growth direction; thin section, polarized light, crossed nicols. E) Sparry calcite cement (arrows) developed between columnar calcite crystals (CC); thin section, polarized light, crossed nicols. F) Isolated rhombohedral crystals (c) growing on aragonite-ray crystals (A); SEM.

scale, these layers commonly are discontinuous and their thickness varies laterally, especially between the axial part and the lateral faces of stalagmite. Along the lateral sides, detrital layers may even disappear below overhanging parts of the stalagmite surface.

Depending on the thickness of the micro-layer, the growth of the underlying carbonate crystals may have been stopped, and nucleation of new crystals occurs on the detrital deposit independently of the orientation of crystals below the discontinuity. In other cases, the

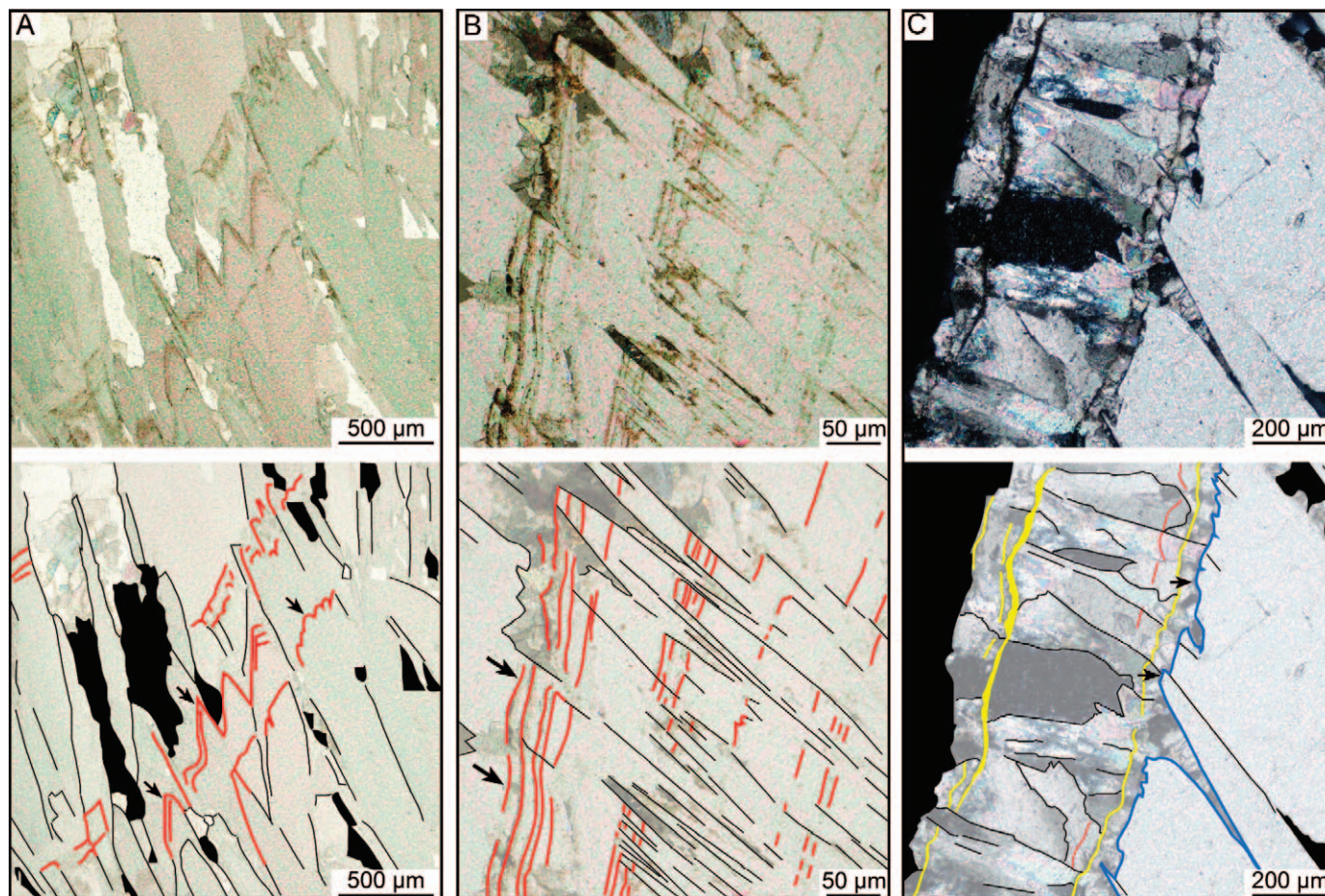


FIG. 6.—Growth surfaces, discontinuities and inclusion levels, microphotographs of thin sections, and associated line drawings. **A)** Successive growth surfaces related to inclusion levels (red lines), some of which (arrows) following former positions of crystal terminations (type 1); polarized light. **B)** Successive growth surfaces related to inclusion levels (red lines); some of these surfaces are associated with dissolution (arrows); polarized light. **C)** Several successive surfaces of discontinuity: growth discontinuity associated with partial dissolution of underlying crystals (blue line) and local deposit of detrital argillaceous sediment (arrows); growth surfaces marked by an argillaceous layer (yellow); thin discontinuous inclusion level (red line); polarized light, crossed nicols.

micro-layer is not thick enough to prevent the growth of underlying crystals completely, and crystalline growth may be disrupted only slightly with crystalline orientation maintained above the discontinuity. A spectrum of intermediate cases, between continuous crystallization and complete interruption of crystal growth, are evident.

Growth Discontinuity Resulting from Change of Crystallization.—This type of growth discontinuity is marked by a major change in crystallization, expressed either by abrupt change in crystal morphology but not mineralogy, or by change in mineralogy. A representative example (Fig. 8C) shows the succession (from base to top, and through time): primary columnar calcite, a discontinuity indicating an interruption of columnar calcite growth, primary aragonite.

Typically, the crystals which precipitate immediately above the discontinuity surface show strongly divergent orientations between neighboring crystals with relatively sparse nucleation sites (Fig. 8C). These features attest to a weak competitive spatial growth between neighboring crystals related to a gradual start-up of crystallization after a growth discontinuity.

Growth Discontinuity Associated with Dissolution.—The growth discontinuity is defined by a truncation of underlying crystals. This truncation is expressed by either 1) blunt crystal terminations or 2) top

surface of crystal terminations upwardly concave, these micro-excavations being underlined by inclusions layers (Fig. 6B, C).

Internal Sediment

Internal sedimentation (i.e., recognized as sediment within pre-existing speleothem porosity) is a discrete process. Internal sediment consists of argillaceous material deposited as geopetals in primary porosity of primary columnar calcite (Fig. 9A). In these samples, these internal sediments typically occur in voids one or more millimeters in width, and are up to 300 micrometers thick. They were not found in the stalactic specimens. The presence of these micro-deposits casts an orange-brown color to stalagmite calcite at the macroscopic scale. Where the internal sediment is deposited over a group of growing calcite crystals, detrital sediment appears to partly fill the lows between crystal tips, and to prevent further crystalline growth at crystal edges. No dissolution features of crystal terminations are evident in thin section. Calcite growth therefore is limited to the upper parts of crystal terminations protruding over the geopetal sediment (Fig. 9B).

Dissolution Features

Dissolution of Aragonite.—Selective dissolution of aragonite occurs at microstructural scale forming micro-irregularities along the faces and

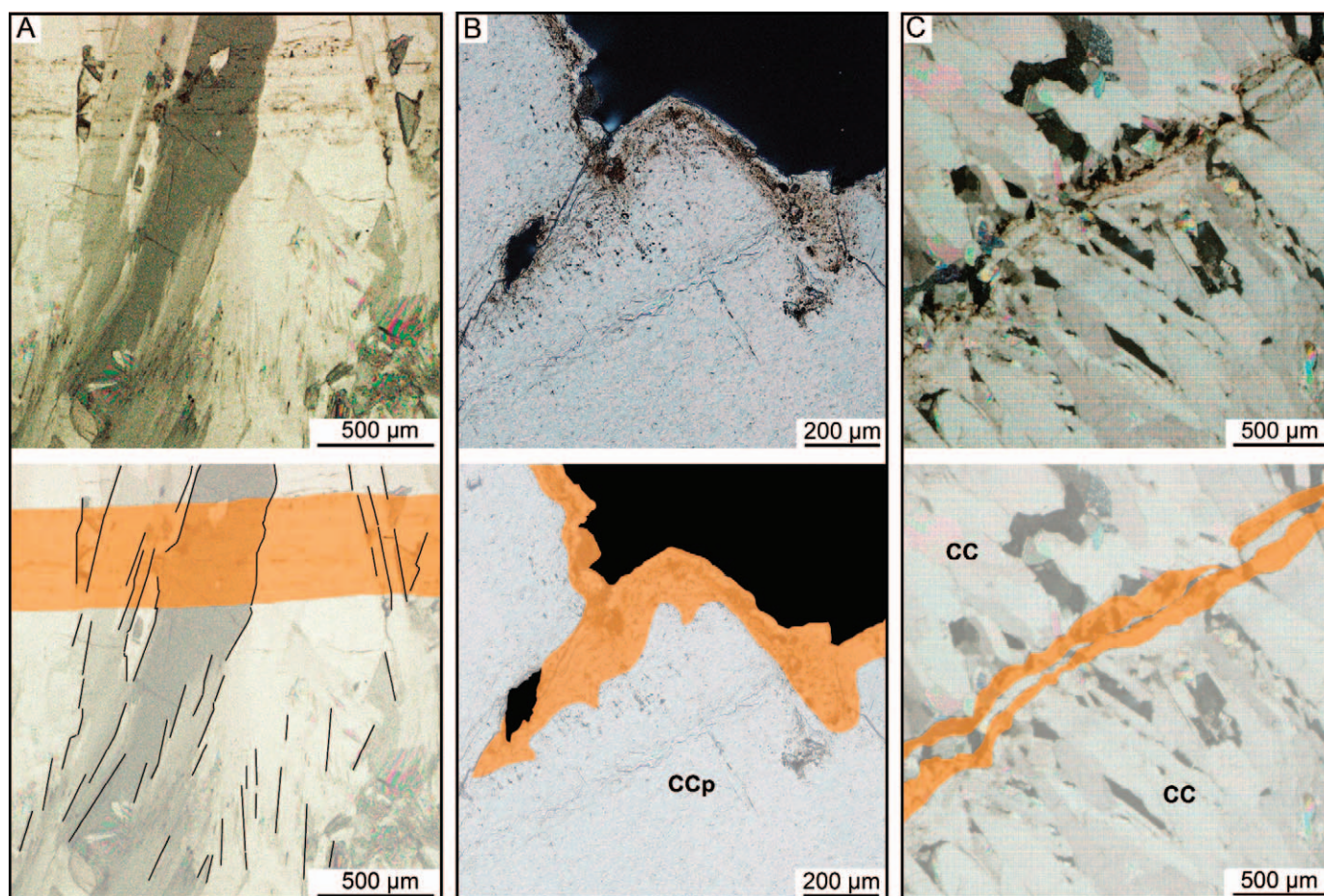


FIG. 7.—Growth surfaces, discontinuities and inclusion levels, microphotographs of thin sections, and associated line drawings. **A)** Successive growth surfaces related to diffuse inclusion levels (type 2 highlighted in translucent orange) and discrete visible inclusions in primary columnar calcite; polarized light. **B)** Crystals of primary columnar calcite (CCp), showing both diffuse and individually distinct micro-inclusions; polarized light, crossed nicols. **C)** Two successive levels of diffuse micro-inclusions (translucent orange); CC, columnar calcite; polarized light, crossed nicols.

terminations of aragonite crystals. Primary ray aragonite with high primary intercrystalline porosity appears particularly susceptible to micro-dissolution (Fig. 9C). Micro-dissolution features along aragonite crystal faces commonly are associated with aragonite–calcite recrystallization zones. They are most common in the transition zone between aragonite and columnar calcite, in areas affected by recrystallization. Micro-dissolution associated with recrystallized zones also is evident clearly along the crystal faces of aragonite precursor relics included in sparitic calcite (Fig. 9D).

Dissolution of Calcite.—Dissolution also affects primary columnar calcite and is initiated preferentially as elongated voids along the boundaries between neighboring crystals (Fig. 10). Such secondary voids are enlarged gradually by the ongoing dissolution process, and their width varies from a few micrometers to a few hundreds of micrometers (Fig. 10C, D). At a further advanced stage, these dissolution voids are connected to each other and form a frame of micro-channels in the central part of the stalagmite (Fig. 10A, B).

Recrystallization Features

Aragonite to Aragonite.—This type of isomineral recrystallization is expressed at the optical-microscope scale by a gradual textural change

from fibrous needle-like aragonite crystals, typically with a fan-like arrangement, to much larger ray crystals (Fig. 11A, B). Relics of needle-like crystals encased in larger ray crystals are evident under SEM (Fig. 11C). In the samples, Raman spectrometry indicates that fibrous and ray crystals both are aragonite, with no shift of Raman bands. Similarly, EDS and WDS analyses of both primary and secondary aragonites have shown no marked difference in elemental composition (Table 2).

Aragonite to Sparry Calcite.—This sparry calcite consists of polygon-like to hexagonal large crystals (several tens to several hundreds of micrometers) with a packed arrangement. The large size of crystals, compared to other crystals forming the Pont-de-Ratz speleothems, gives these recrystallized zones a more translucent aspect in the slabs. Recrystallization is demonstrated by the common presence of relic crystals of aragonite included in the sparry calcite (Fig. 11D–F). Where the sparry crystals are of large size (several hundreds of micrometers) and the relics are abundant, the former fan-like arrangement of acicular aragonite is still visible in places (for example, at the bottom left of Fig. 11E).

In the samples, the aragonite mineralogy of the precursor has been demonstrated directly using Raman spectroscopy. Although the spatial resolution of the EDS and WDS microprobes does not allow the analysis

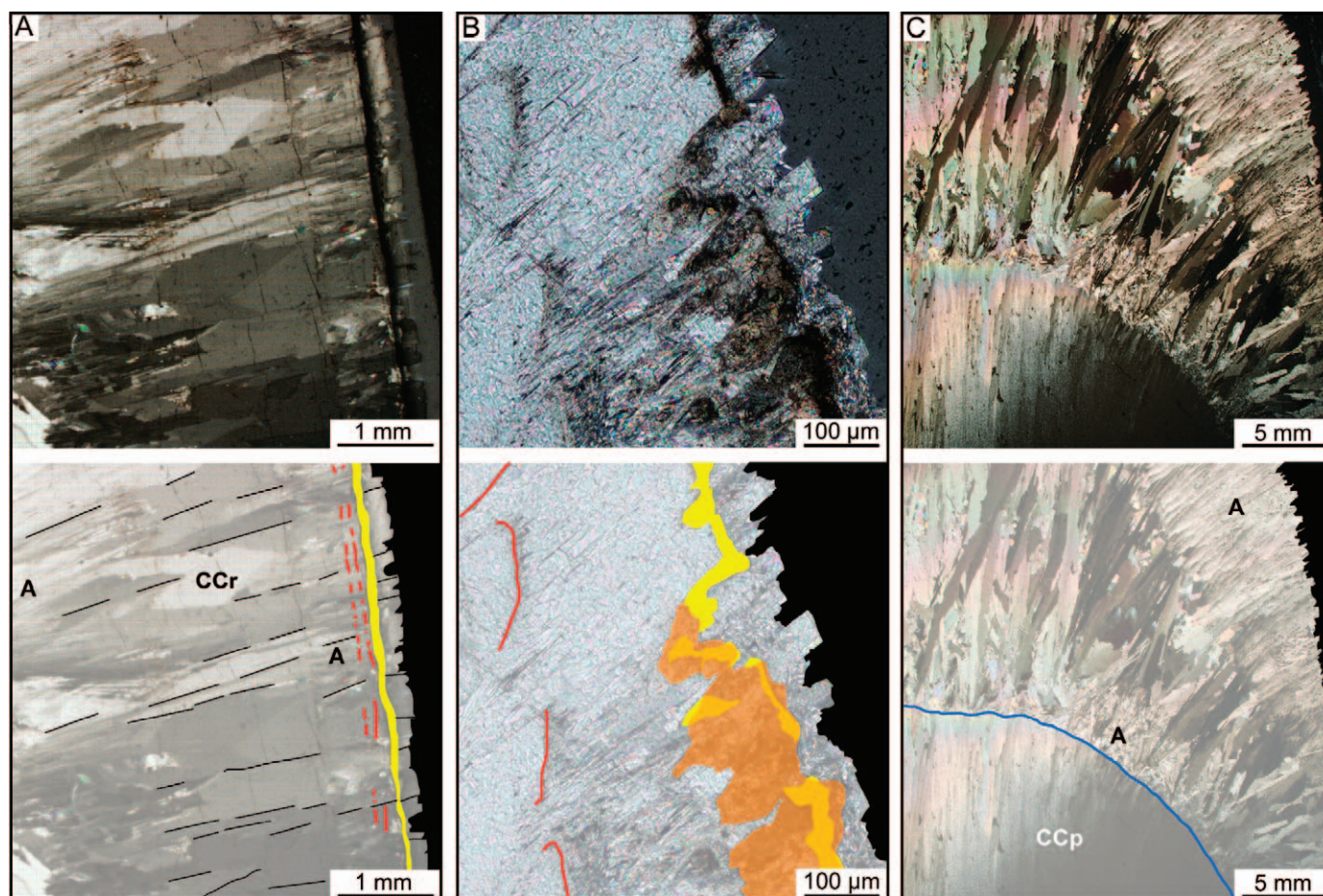


FIG. 8.—Growth surfaces, discontinuities and inclusion levels, microphotographs of thin sections, and associated line drawings. **A)** Two successive growth surfaces marked by discontinuous inclusion levels (red lines), and one later growth discontinuity underlined by a continuous argillaceous micro-layer (yellow); A, aragonite, CCr columnar calcite resulting from recrystallization of former aragonite; polarized light, crossed nicols. **B)** Discontinuous inclusion level (red lines) followed by a growth discontinuity formed by a diffuse inclusion level (translucent orange) and the deposit of a discontinuous argillaceous micro-layer (yellow); polarized light, crossed nicols. **C)** Growth discontinuity resulting from change of crystallization (blue line); CCp, primary columnar calcite; A, aragonite; polarized light, crossed nicols.

of single relict crystals with confidence, results show a variable but elevated content of Sr (450–1500 ppm) for the areas bearing precursor relics, and areas richer in aragonite relics have higher Sr content (about 800–1000 ppm). Otherwise, the Mg content of the sparry calcite is below 600 ppm. In large sparry crystals, several spot analyses within single calcite crystals can be assessed to evaluate variability of trace-element content in different parts of the crystals. For each sparry crystal, analytical spots were placed at successive positions between the center and the periphery of the crystal, and avoiding relics of the aragonite precursor within the spot area. These results show Mg values below detection limit on the crystal margins and highest values in the internal parts of individual crystals (Fig. 12A, B). This result is interpreted to reflect fine-scale precipitation of calcite during the recrystallization process that induces slight changes in the elemental composition of the fluid from which carbonate forms.

Aragonite to Columnar Calcite.—Aragonite may also recrystallize into columnar calcite. This columnar calcite is very similar to the primary columnar calcite. It therefore is not possible to distinguish at first glance primary and secondary columnar calcites based on the sole morphology and arrangement of crystals, although in the samples, the recrystallized columnar crystals tend to be slightly larger than the primary columnar crystals.

Macroscopically, recrystallization is shown clearly in slab hand sample either by islets of acicular aragonite fans, with a white satin-like aspect, isolated in an area of translucent calcite (Fig. 13A), or by fibrous aragonite laterally passing to calcite in the same growth layer (Fig. 13B). Observations of thin sections show relics of aragonite crystals encased in columnar calcite, attesting to the secondary origin of calcite (Fig. 13C, D). However, relics in the recrystallized columnar calcite are much less frequent than relics in sparry calcite, making the establishment of the calcite origin difficult. Both primary and secondary aragonite can recrystallize into columnar calcite.

Analysis of the Mg content of the recrystallized columnar calcite with the WDS microprobe reveal an average of 7848 ppm, but variability between 5278 and 12,483 ppm. It is therefore slightly higher than the primary columnar calcite (Table 2).

Detailed observations of aragonite–columnar calcite recrystallized zones were made in areas composed mainly of aragonite, i.e., still at an early stage of recrystallization. In these zones, aragonite is represented by large-size ray crystals (100–200 micrometers wide and several hundreds of micrometers long) with different orientations between neighbors, and thus preserving intercrystalline porosity. Backscatter electronic microscopy (BSE) shows some scattered elongated crystals of columnar calcite in these zones (Fig. 14): the calcite crystals appear slightly darker gray on

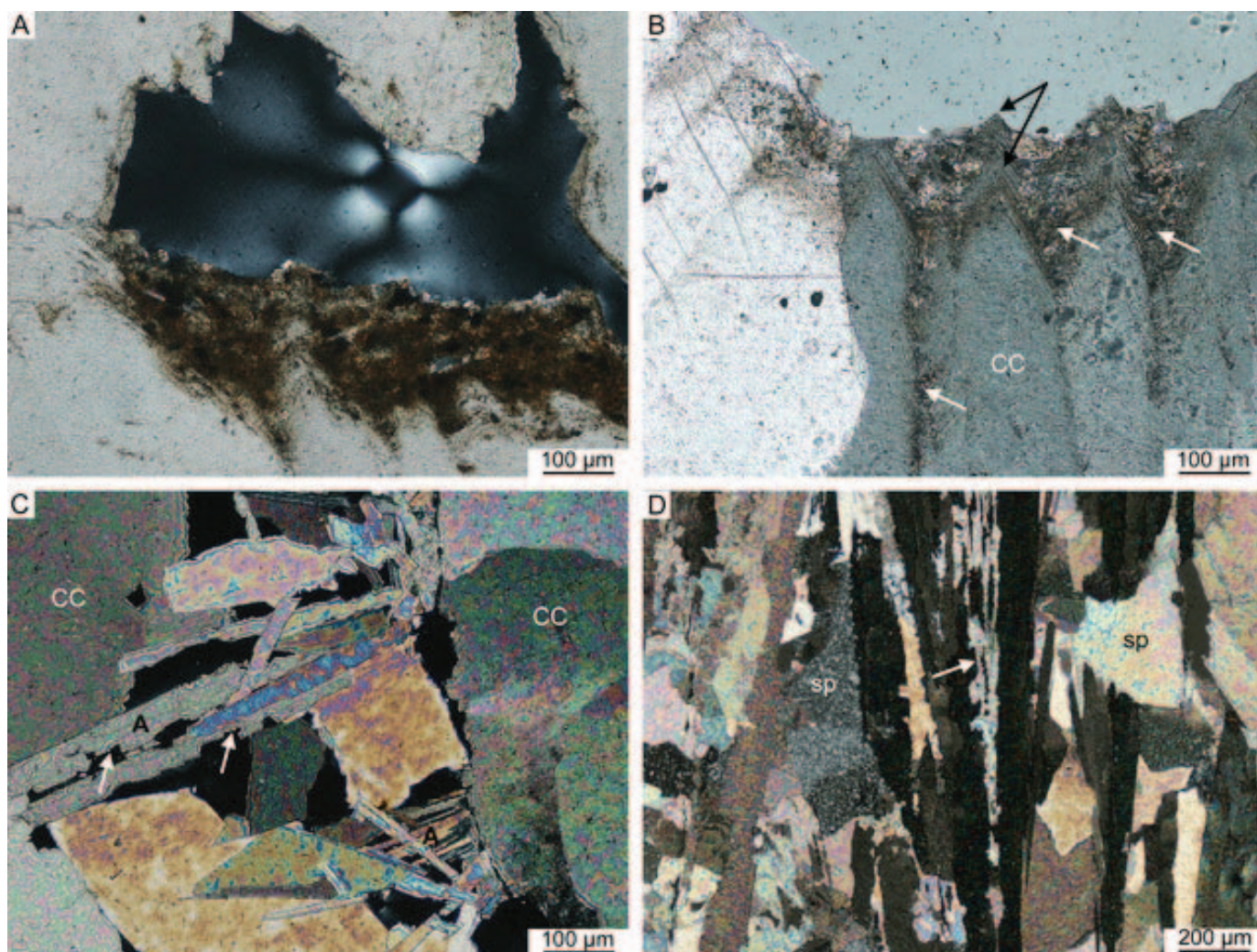


FIG. 9.—Internal sediment and dissolution of aragonite; thin section, polarized light, crossed nicols. A, B) Internal sediment, axial vertical growth direction of the stalagmite is oriented toward the top of microphotographs. A) Internal geopetal argillaceous sediment deposited in a primary void open in primary columnar calcite. B) Internal sediment deposited in primary void and crystal termination of the primary columnar calcite protruding over the geopetal sediment surface, detrital sediment deposited in the valleys between crystal tips (white arrows), successive crystal tips showing continuous growth (black arrows). C) Partial dissolution of primary ray aragonite (arrows), A, aragonite, CC, columnar calcite. D) Partial dissolution (arrow) of precursor aragonite relics included in sparitic calcite (sp).

the backscattered images (due to their higher Mg content as shown by the EDS spot analyses) compared to the aragonite crystals. In the same zones, SEM images revealed the presence of small isolated rhombohedral calcite crystals developed on the surfaces of aragonite ray crystals (see description above and Fig. 5F).

Analyses of these calcite rhombohedrons indicate that they have the same Mg values as that of columnar calcite (Table 2). This observation, together with the exclusive occurrence of these crystals in areas at an early stage of recrystallization (Figs. 5F, 15), suggests that the isolated rhombohedral calcite cementation represents the initiation process prior to recrystallization of aragonite ray crystals into columnar calcite (Fig. 15A, B). Following this early step (Fig. 15B, C), recrystallization gradually takes place. The fluid from which these early rhombohedral crystals developed is undersaturated against the aragonite crystals, as a result of decreasing supersaturation. Aragonite became unstable and crystals are completely or partially dissolved, leading in the latter case to the formation of scarce aragonite relics enclosed in calcite. The process occurs through growth of these seed crystals both towards the interior of the precursor crystal of aragonite, which is progressively dissolved as

recrystallization proceeds, and on the previous external surface of the precursor (Fig. 15C). On this surface, competitive growth between seed crystals tends to favor the development of individual crystals of similar orientation and their gradual aggregation into large crystals of columnar calcite, resulting in a marked decrease of primary intercrystalline porosity (Fig. 15D).

DISCUSSION

Distinguishing Primary and Secondary Features and Processes

Among the various products and processes described above, some are directly involved in the development of the speleothem (i.e., “spelean growth history”), whereas others are related to modifications of a pre-existing spelean structure (i.e., “spelean diagenetic history”). It is therefore fundamental to distinguish between events, processes, and products, participating in the stalagmite growth (i.e., primary crystallization, growth discontinuities, etc. that we group in the category “spelean growth history”), and those modifying the properties of already existing products below the growing external surface (i.e., recrystallization,

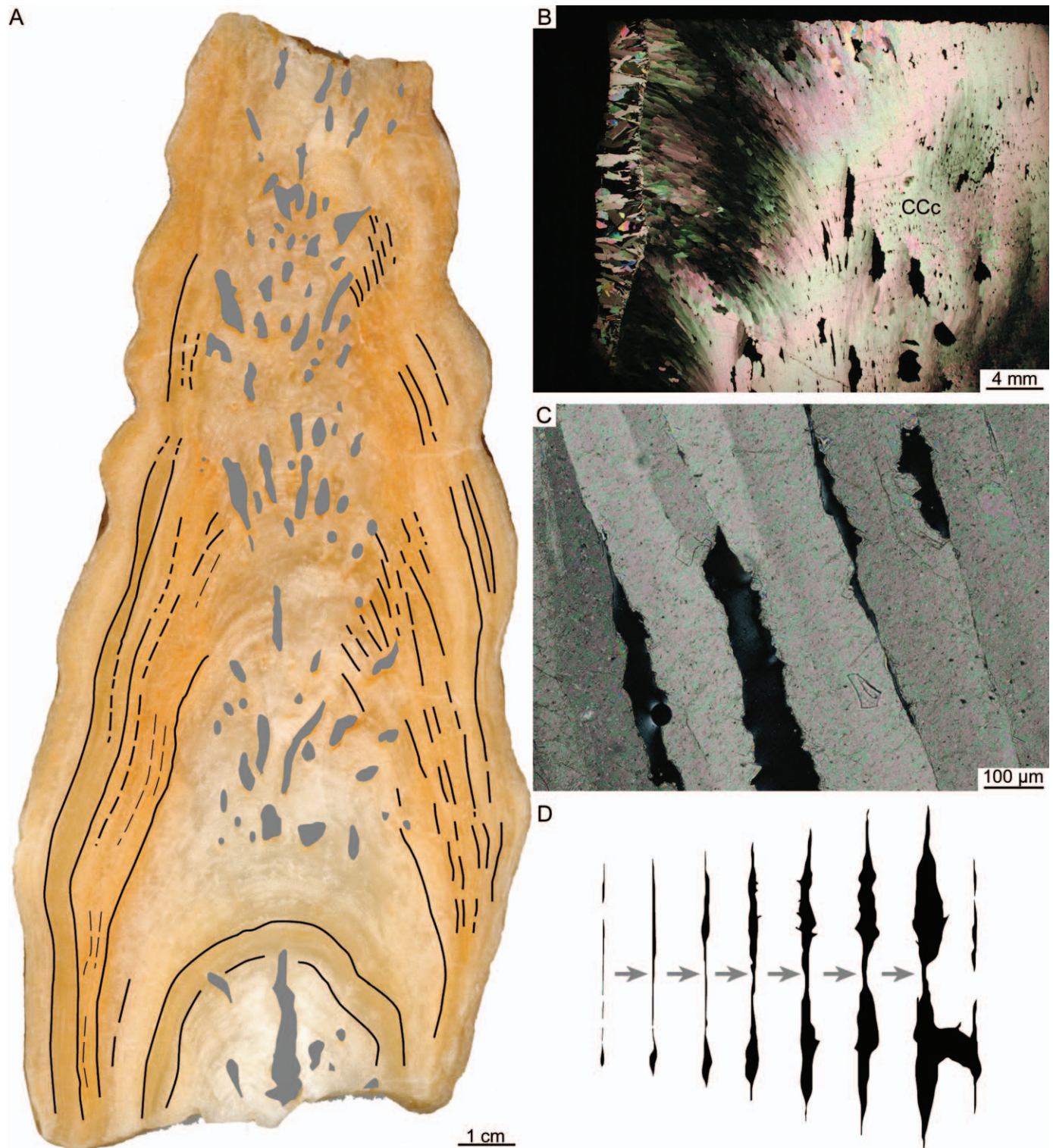


FIG. 10.—Character of calcite dissolution. **A)** Slab of a stalagmite composed mainly of primary columnar calcite, in reflected light. Growth banding is overlined in black; pores, shown in gray, are concentrated in the central part of the speleothem. **B)** Primary columnar calcite (CCp) forms the central lower part of a stalagmite and shows numerous large and small voids; thin section, polarized light, crossed nicols. **C)** Closer view of the primary columnar calcite with dissolution voids preferentially open at the boundary between neighboring crystals; thin section, polarized light, crossed nicols. **D)** Sketch illustrating the gradual opening of secondary voids in the primary columnar calcite.

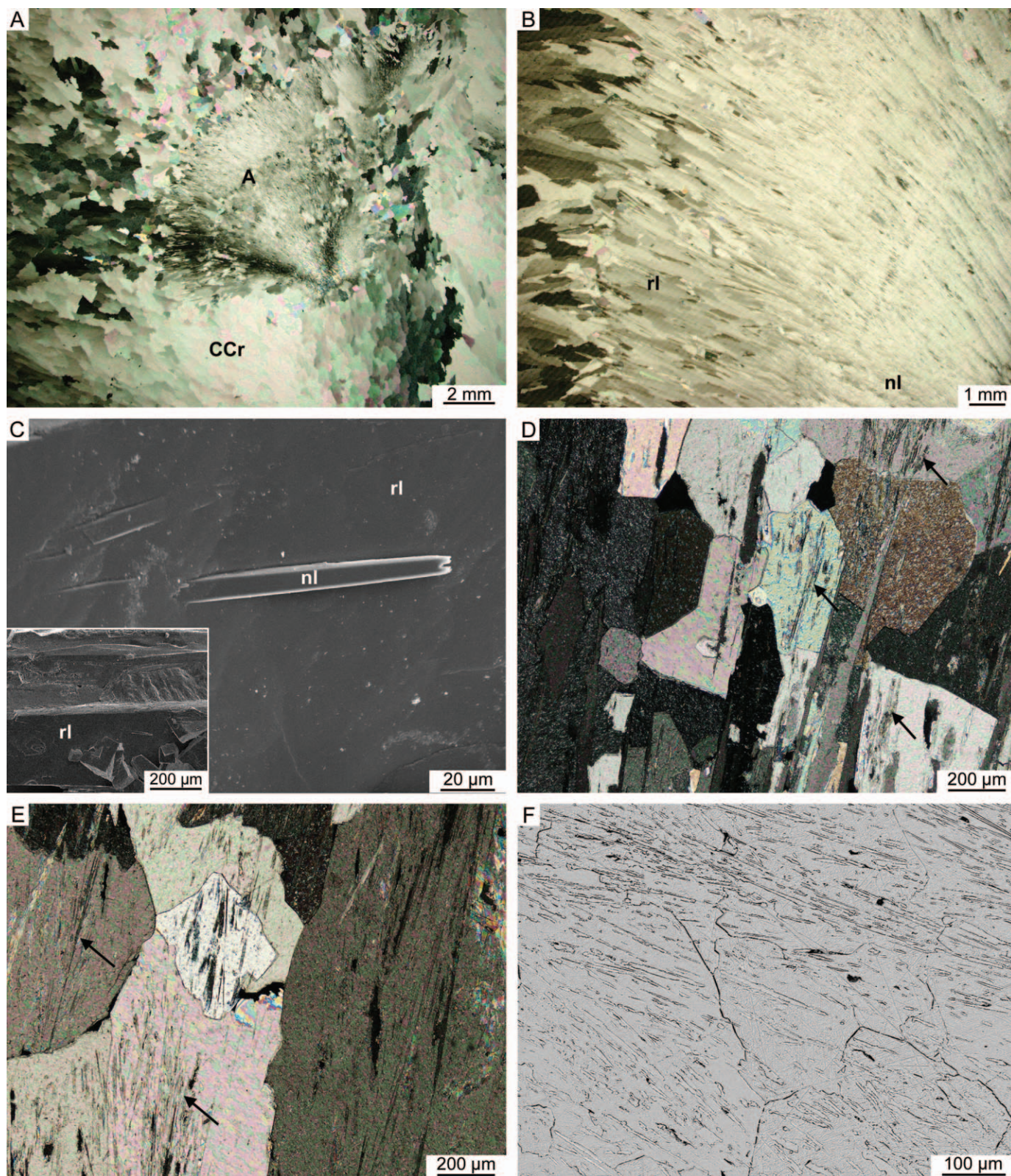


FIG. 11.—A–C) Representative features associated with recrystallization, aragonite–aragonite. **A)** Patchy residual area of aragonite (A) within secondary columnar calcite (CCr); thin section, polarized light, crossed nicols. **B)** Closer view of the residual area of aragonite seen in part A, showing typical aragonite–aragonite recrystallization characterized by a gradual textural change from needle-like (nl) to larger ray (rl) aragonite crystals; thin section, polarized light, crossed nicols. **C)** Relics of needle-like primary aragonite (nl) included in a ray secondary aragonite (rl), inset showing a larger view of the same area with ray (rl) aragonite crystals and small rhombohedral crystals of calcite cement; SEM (SE). D–F, Representative features associated with recrystallization, aragonite–sparry calcite. **D)** Relic crystals of aragonite (arrows) included in large polygonal crystals of sparry calcite; thin section, polarized light, crossed nicols. **E)** Relic crystals of aragonite (arrows) included in sparry calcite; the former fan-like arrangement of acicular aragonite is still visible in some places (half bottom left); thin section, polarized light, crossed nicols. **F)** Polygonal crystals of sparry calcite showing numerous relic crystals of acicular aragonite; SEM (BSE).

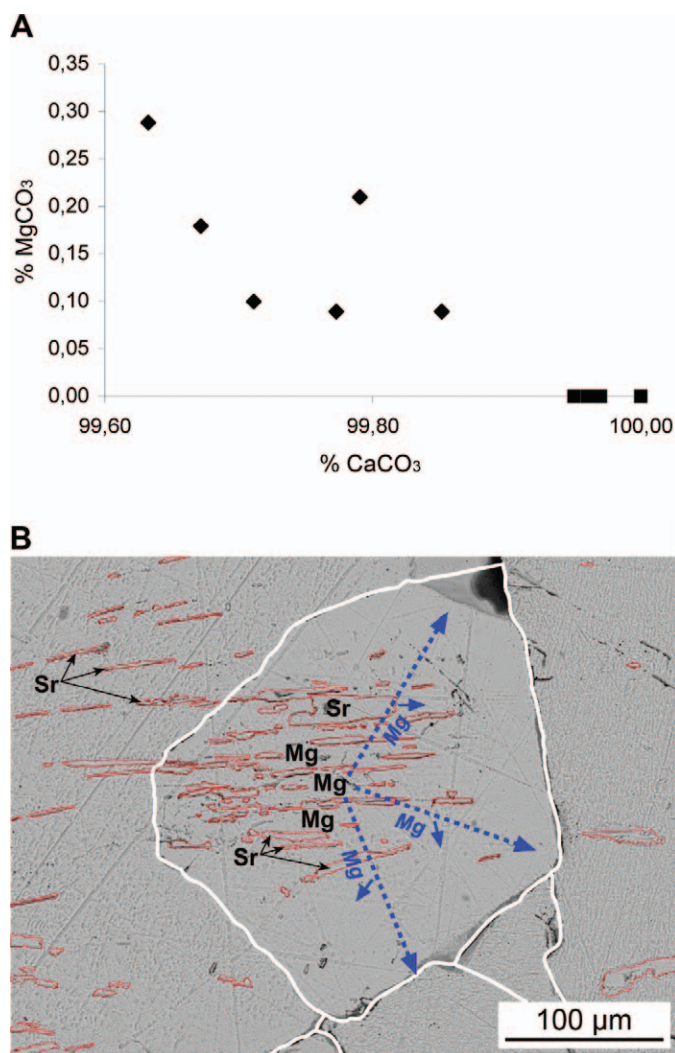


FIG. 12.—A, B) Representative features associated with recrystallization of aragonite into sparry calcite. **A)** Results of WDS microprobe analyses of individual crystals of sparry calcite with aragonite relics; analyses were performed in sparite areas between relics; diamonds, internal parts of crystals with slight Mg content; square, margins of crystals with no detectable Mg. **B)** Example of Mg and Sr distribution in sparry calcite resulting from recrystallization of acicular aragonite, SEM image. Numerous relics of precursor aragonite (surrounded by red lines) encased in large polygonal sparry calcitic crystals (surrounded by white lines). Aragonite relics are Sr rich (several hundreds to one thousand ppm). The Mg content of calcite tends to be higher in the central part of calcite crystal, where relics are more numerous than close to the calcite crystal margins, whereas Mg is not detectable with the microprobe.

cementations in the deep parts of the stalagmite, etc., that we group in the second category, “spelean diagenetic history”). The purpose of such an exercise is not to establish a dating chronology between events, since it is not possible in practice, for example, to date, with radiometric techniques, recrystallization phases. The objective is instead to identify primarily formed features and those resulting from subsequent modifications.

Although both groups of processes are controlled by environmental factors, the first can easily be replaced in a sequential order within spelean growth by establishing paragenetic sequences of primary precipitates integrated in the “stratigraphical” frame provided by the architecture of stalagmite. Processes belonging to the second group, because they modify pre-existing spelean material at various depths below the external surface of the speleothem, lead to resulting products having properties in part

“inherited” from precursor material (through relics for example) and in part newly acquired characters. As such, these sorts of features can be more difficult to place in a general temporal frame. Nonetheless, a clear distinction between both types of processes is a fundamental step in the understanding of the stalagmite material and therefore a prerequisite before attempting to reconstruct environmental or climate history from spelean material or before applying radiometric dating techniques. This concept has been expressed by several authors (Cabrol 1978; Frisia et al. 2002; Railsback et al. 2002), but it is not applied systematically in many studies. For example, in the case of the Pont-de-Ratz speleothems, it appears crucial to know the origin of the columnar calcite, either primary or secondary (resulting from recrystallization of aragonite) before dating it.

Different features of the Pont-de-Ratz are driven by one or the other group of processes (Table 4). Whereas processes such as recrystallization or internal sedimentation are obviously related to the diagenetic history of the speleothem, dissolution may take place either at the speleothem external surface (e.g., Fig. 6B) and, hence, be part of its growth history, or occur as a later process affecting deeper parts of the spelean material (e.g., Fig. 10A, C, D).

Significance of Growth Surfaces, Discontinuities, and Inclusion Levels

Growth Surface Related to One or Several Inclusion Levels.—These inclusion horizons are related to events favoring the input of colloidal particles transported either by the drip water (Hartland et al. 2012) or aerosols transported by air circulation in the cave (Dredge et al. 2013). Correlation of such events between stalagmite samples is difficult, in particular because both the amount of colloidal particles or aerosols being deposited on a given stalagmite surface and their efficient incorporation in the crystals by the advancing growth surface are influenced strongly by local environmental factors, such as variations of drip rate. For example, different drip rates between stalagmites may influence the amount of aerosol particles incorporated at the upper surfaces of growing stalagmites (Dredge et al. 2013), even leading to different records of the same event in neighboring speleothems. Additionally, the thin layer of colloidal particles or aerosols deposited at the top of the stalagmite may be washed away by a marked increase of drip rate or a restart of drip after a stop, resulting also in differences of record between individual specimens.

Growth Surface Marked by a Detrital Layer.—The detrital material consists mainly of clay, with possible contribution of particulate and colloidal organic matter (similar to Hartland et al. 2012) or aerosols or dust (e.g., Berthaux et al. 2002; Dredge et al. 2013; Railsback et al. 2013). Since these layers may be discontinuous or vary laterally in thickness, they are not necessarily related to growth interruption of the stalagmite, but suggest a decrease of drip water flow allowing fine-grained material to be deposited on the stalagmite surface.

Growth Discontinuity Resulting from Change of Crystallization.—The growth interruption directly results from a change in the supply of drip water feeding the stalagmite (decrease or stop of drip water, lower intensity of degassing, or both). Another potential line of evidence of an environmental event is growth surfaces marked by a mineralogical change of precipitate (Fig. 8C), which may reflect a major modification of drip water chemistry or drip rate. Mineralogical shift from calcite to aragonite precipitation in speleothems has been explained by an increase in Mg²⁺ concentration in the water film flowing at the surface of stalagmite and beyond, related to climatic change towards aridity (Railsback et al. 1994; Frisia et al. 2002; McMillan et al. 2005; Wassenburg et al. 2012). In the stalagmites of the Pont-de-Ratz Cave, such a mineralogical shift from calcite to aragonite in precipitates would be expressed by a marked

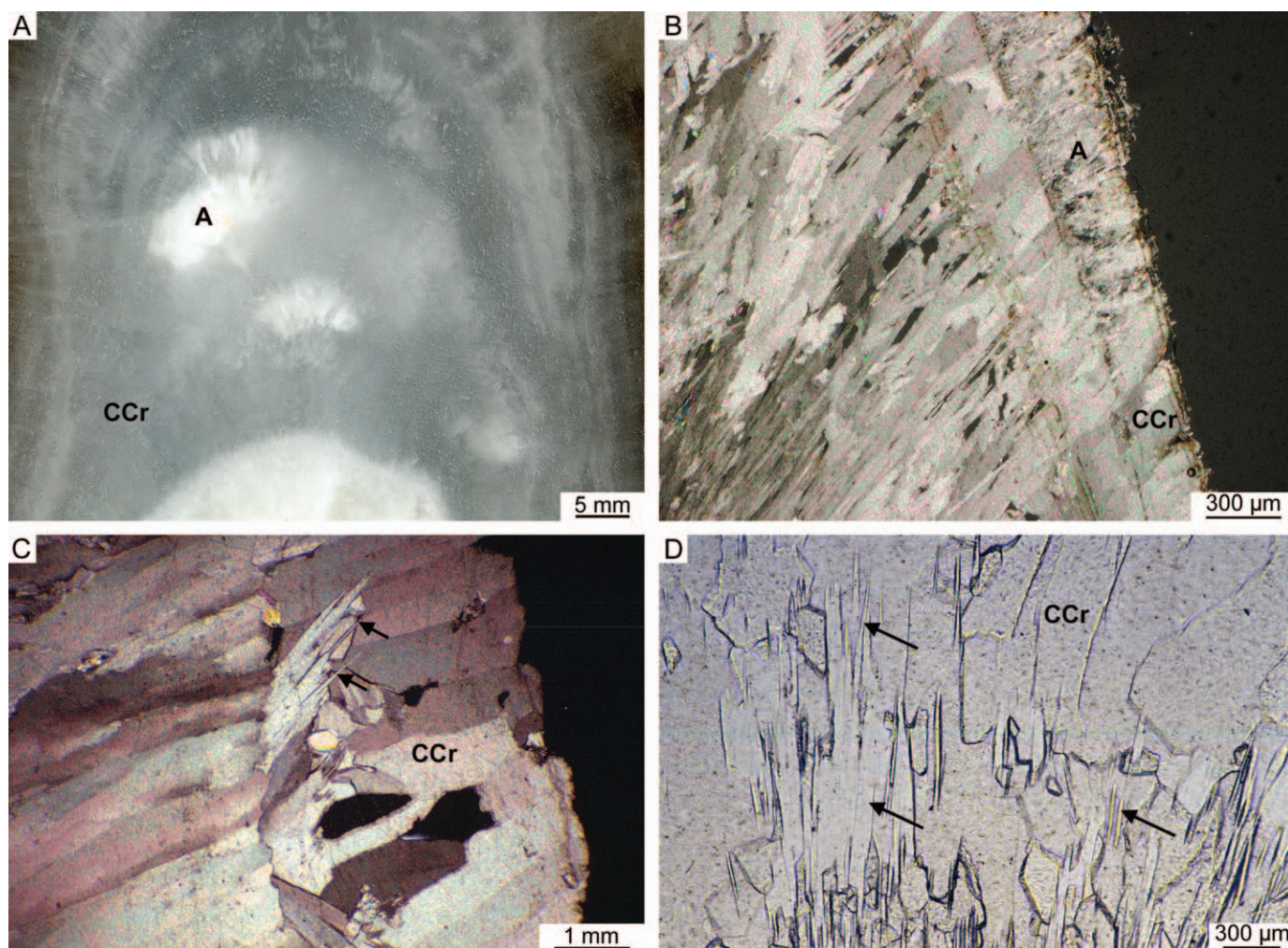


FIG. 13.—Representative features associated with recrystallization, aragonite–columnar calcite. **A**) Relic islets of acicular aragonite (A) within translucent area of recrystallization columnar calcite (CCr), part of stalagmite slab seen in reflected light. **B**) Area at various stages of recrystallization. The younger layer shows small aragonite fans (A) laterally passing into columnar calcite (CCr); thin section, polarized light, crossed nicols. **C**) Relics of acicular aragonite crystals (arrows) encased in recrystallization columnar calcite (CCr); thin section, polarized light, crossed nicols. **D**) Numerous relics of acicular aragonite crystals (arrows) included in secondary columnar calcite (CCr); thin section, polarized light.

increase in Sr/Ca ratio (since our results show that the Sr content in primary aragonites is about ten-fold the Sr content in primary columnar calcite; see Table 3) and a strong decrease in the Mg/Ca ratio of the carbonate crystals (see Table 2). Conditions favoring the precipitation of the unstable polymorph aragonite (instead of calcite) commonly include an increase of the Mg/Ca ratio in the cave drip water (Cabrol 1978; Harmon et al. 1983; and references cited above). This change in turn can be favored by a decrease in drip water recharge in combination with enhanced evaporation rate in the cave atmosphere or by a prolonged degassing resulting in “prior calcite precipitation” occurring in the epikarst, which depletes the water entering the cave in Ca^{2+} ions since the repartition coefficient of Mg in calcite is < 1 . Mg^{2+} cations adsorbed on specific nucleation sites prevent the growth of calcite crystals, and represent one of the most common calcite inhibitors (Rowling 2004; De Choudens-Sanchez and Gonzalez 2009; Hopley et al. 2009; Martin-Garcia et al. 2009; Martin-Pérez et al. 2012), although other ions such as Zn^{2+} or Pb^{2+} have been reported as efficient calcite inhibitors in relatively wet climatic conditions (Caddeo et al. 2011). In addition, other important factors such as configuration of the water circulation in the karst aquifer and residence time of water in the epikarst, carbonate concentration and

pH of drip water, together with the mineralogy of the bedrock which provides the Mg content, also influence the mineralogy of spelean precipitates. In the case of the Pont-de-Ratz Cave, the nature of the bedrock (dolomite and dolomitized limestone) appears as the most efficient source of Mg^{2+} ions in water feeding the stalagmites.

Growth Discontinuity Associated with Dissolution.—This type of surface expresses an interruption of stalagmite growth accompanied or rapidly followed by dissolution of underlying carbonate crystals. The shift from crystallization to growth interruption and then to dissolution of carbonate crystals implies a change in the quality of drip water, the water feeding the stalagmite becoming undersaturated with respect to calcium carbonate.

In particular, micro-scale dissolution occurring along growth discontinuities (Fig. 6B, C) in stalagmite samples can be interpreted as a result of condensation of undersaturated or acidic waters with high values of pCO_2 on former external surfaces of the stalagmite. This process has been described widely under the terms “condensation-corrosion” (Dublyansky and Dublyansky 1998). The term “corrosion” obviously is not appropriate in this case, because it refers to partial dissolution of

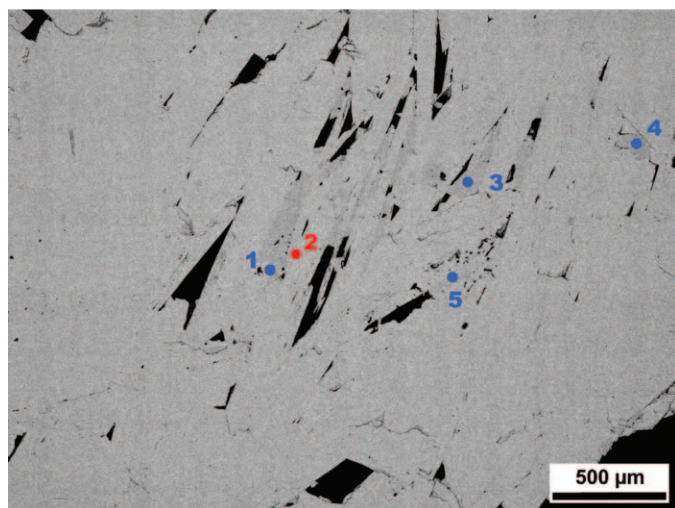


FIG. 14.—Representative features associated with recrystallization, aragonite-columnar calcite, early stage of process. (BSE) SEM view of an area at an early stage of recrystallization and associated EDS spot analyses. Zones with detected Mg correspond to columnar calcite crystals and appear slightly darker gray on the backscattered image. EDS spots are indicated by blue (Ca and Mg content detected) and red (only Ca content detected) dots.

carbonate minerals. The term “corrosion” in its strict sense means oxidation of a metal, and hence cannot be applied to the dissolution of calcium carbonate. For this reason, the terms “partial dissolution” or “microdissolution,” which commonly are used in carbonate diagenetic

studies, are more appropriate and are unambiguous. These processes occur when air equilibrating with cave atmosphere produces condensed moisture over the cave walls and speleothems. Condensation is produced when the temperature of cave walls and speleothem surfaces is below the air dewpoint and forms a water film in equilibrium with the CO_2 partial pressure of the cave atmosphere (Sarbu and Lascu 1997; Dreybrodt et al. 2005; Audra et al. 2007; Martin-Pérez et al. 2012). Such moisture is acidic or undersaturated with respect to calcium carbonates due to the presence of CO_2 , causing partial dissolution of bedrock and speleothems at various spatial scales. Such processes are strongly dependent on air circulation patterns in the cave, and hence exchanges with external environment and the overall cave configuration (Tarhule-Lips and Ford 1998; Auler and Smart 2004; de Freitas and Schmekel 2006). Surface discontinuities associated with such dissolution features therefore provide evidence of past events causing changes in cave air circulation. Such events, however, can act at a large range of spatial scales from regional (in relationship with elevations of caves and individual karst massifs) to the scale of individual speleothems (e.g., see Dublyansky and Dublyansky 1998 for a review). An alternative explanation of such features has been reported by Railsback et al. (2011), who described surfaces of discontinuity accompanied by dissolution in a stalagmite from NW Spain. In this work, calcite dissolution was related to a change to rapid drip rate, which prevented sufficient degassing to bring feeding water to equilibrium with CaCO_3 , and hence produced dissolution at the surface of the stalagmite (Railsback et al. 2011; Railsback et al. 2013). Given that there is no way to obtain direct information about air paleocirculation in the cave and related rate of degassing, and also that present-day air circulation and chemistry of present-day drip water are not representative of what was happening when these growth discontinuities associated with dissolution

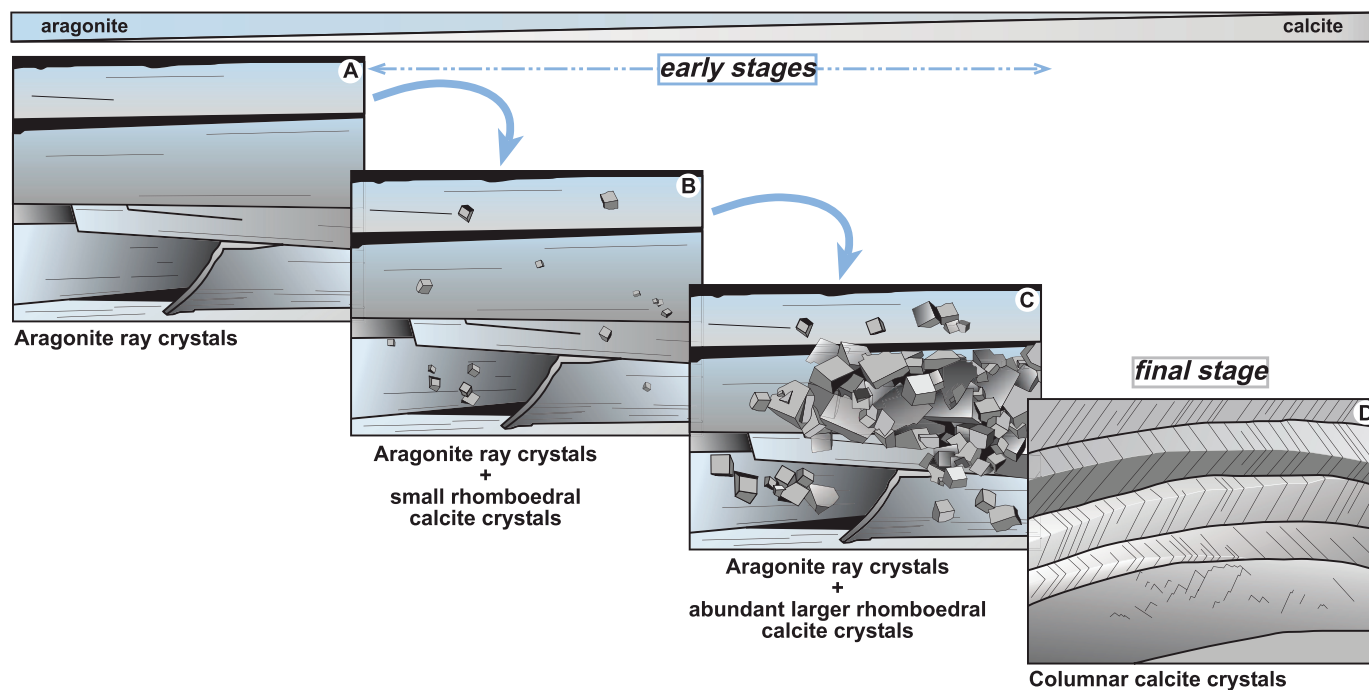


FIG. 15.—Interpretive sketch of successive steps involved in the process of aragonite recrystallization into columnar calcite; sketches redrawn from SEM images. A–C Early stages. **A)** Aragonite ray crystals resulting either from direct precipitation or from a previous recrystallization from fibrous aragonite. **B)** Discrete precipitation of small calcite rhombohedrons on aragonite ray crystals. **C)** Rhombohedral calcite crystals invade the surface of aragonite crystals until these are entirely covered by calcite. Concomitantly, dissolution of aragonite is beginning because waters favoring calcite precipitation are aggressive with respect to aragonite. As the reaction proceeds, further growth of calcite rhombohedrons associated with spatial competition between individual crystals gradually leads to the development of much larger crystals of columnar calcite. Recrystallization process gradually takes place through a microscale thin water film where dissolution of aragonite and precipitation of calcite occur leading to columnar calcite crystals having the same Mg content as the earlier rhombohedral calcite crystals, and encasing rare aragonite relics. **D)** Final stage, consisting of large crystals of columnar calcite with low intercrystalline porosity.

TABLE 4.—Distinction of processes and related products with respect to their link with speleothem growth history or diagenetic history.

Process	Type of Product	Group of Processes		Remark
		Spelean Growth History	Spelean Diagenetic History	
Crystallization on external surfaces	Primary aragonite			
	Primary calcite	+		
	Calcite cement	+		
Cementation	Primary calcite	+		
	isolated rhomboedral crystals		+	
	sparite cement		+	1 st step recrystallization ray aragonite → columnar calcite developed in intercrystalline voids of a pre-existing structure
Growth discontinuities and inclusion levels	Growth surface related to one or several inclusion levels	+		
	Growth surface marked by a detrital layer	+		
	Growth discontinuity resulting from change of crystallization	+		
Internal sedimentation	Growth discontinuity associated with dissolution	+		
	Internal geopetal deposit			
	Secondary porosity			
Dissolution	from dissolution of aragonite		+	
	from dissolution of calcite		+	
	ray aragonite		+	
Recrystallization	sparitic calcite		+	
	columnar calcite		+	
			+	this excluding dissolution linked to growth discontinuity (see above)

features were forming, one can only speculate about the possible mechanisms that produced them.

Diagenetic Evolution of Stalagmites

Diagenetic Evolution through Time.—Inference of temporal scales are a broad but delicate issue in diagenetic studies. The minimum length of time necessary for diagenetic modification depends on several factors, such as the composition of diagenetic fluids and their recharge rates, which are both particularly difficult to quantify. The possible time frame for aragonite–calcite recrystallization in the freshwater vadose zone has been estimated by a few authors, with various timescales on the order of 10^5 – 10^6 years (Morse and Mackenzie 1990) or of less than 10^3 years (Frisia et al. 2002), whereas calcite–calcite recrystallization has been documented to occur within even shorter time (less than one year, Melim and Spilde 2011). Our data indicate that all processes involved in the deposition of the speleothem specimens, together with the processes responsible for their postdepositional evolution, took place during the Holocene, during the last 8000 years.

Complete characterization of the succession of diagenetic processes through time is difficult to establish at the scale of individual speleothems (sample scale). However, suites of diagenetic processes occurring sequentially can commonly be identified from petrological analysis of samples and reconstruction of paragenetic sequences. In the samples from the Pont-de-Ratz Cave, one of the earliest diagenetic processes appears to be the recrystallization of primary acicular aragonite into ray aragonite (Fig. 11A–C). In a diagenetic sequence, petrographical relationships between precursors and recrystallization products reveal aragonite–aragonite recrystallization as the first process. This process is followed by a suite of coupled recrystallizations: acicular aragonite–ray aragonite followed by ray aragonite–columnar calcite (Figs. 11A, 13A).

Spatial distribution of diagenetic products at individual sample scale show that: 1) the same diagenetic process can occur repeatedly several times during the speleothem history (see for example Fig. 5D, where sparry calcite cement occurs at several stratigraphical levels in the stalagmite), 2) there is no direct correlation between intensity of diagenesis (volume of material modified by alteration) and age of the spelean material considered. In other words, the oldest parts of a stalagmite sample are not necessarily the most intensely affected by diagenesis.

Diagenetic Evolution through Space in the Speleothem: Spatial Distribution of Diagenetic Products in Individual Stalagmites.—Diagenetic evolution of any geological material is controlled by the chemistry of diagenetic fluids and the chemical (*sensu* mineralogical) and physical (mainly porosity and permeability) properties of this material. Hence, beside the chemistry of diagenetic fluids, diagenetic evolution of speleothems is strongly controlled both qualitatively (i.e., type of process) and quantitatively (i.e., intensity of diagenesis or amount of modified material) by the mineralogy and chemistry of the original spelean material and also by its microporosity (voids) and permeability (connections between voids). The original mineralogy, geochemistry, and physical properties of the speleothems, together with the nature and origin of the diagenetic fluids (percolating water, condensation, etc.) interacting with the spelean material, influence the spatial distribution of the resulting secondary products at the scale of individual stalagmites.

Two potential sources of fluids can interact with the existing spelean material within a stalagmite. These are: 1) the drip water percolating from the cave ceiling and forming a thin water film, which develops along the stalagmite lateral sides, and 2) the humidity and condensation, which can create a discontinuous water film on the external stalagmite surface. In both cases, a small amount of water can also migrate by capillarity towards the interior of the speleothem, following surfaces of interstitial

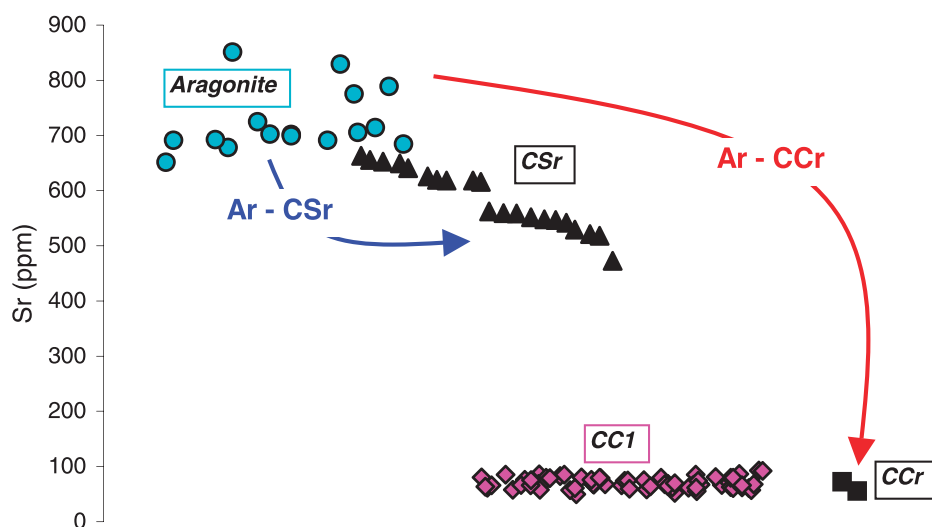


FIG. 16.—Impact of aragonite-calcite recrystallization on the Sr content and effect of the analytical sampling size on the apparent inheritance of precursor geochemical signature (measures P-XRF, detection limits and spatial resolution provided in text “Methods and Material”; horizontal axis represents categories, no scale). Primary aragonite crystals (blue dots) have the highest Sr content. Their recrystallization into columnar calcite (red arrow) occurs with an important decrease of Sr (secondary columnar calcite, CCr, represented by black squares). Primary columnar calcite crystals (CC1, pink diamonds) have about the same Sr value as the columnar calcite resulting from recrystallization of aragonite (black squares). Zones with recrystallization of aragonite into sparry calcite (blue arrow) have Sr values lower than primary aragonite but much higher than the columnar calcite, due to the presence of aragonite relics in the large sparry calcite crystals (CSr, black triangles).

pore walls or contact surfaces between neighboring crystals. Depending on the chemistry of this water and its degree of saturation with respect to the carbonate minerals with which this water interacts, diagenetic modifications (i.e., cementation, recrystallization, and dissolution processes) may occur at different levels below the external surface of the stalagmite.

Recrystallization Processes

Aragonite–Aragonite.—This recrystallization occurs through gradual textural changes from needle-like aragonite to much larger ray aragonite crystals (Fig. 11A, B). The recrystallization process is demonstrated by 1) the lateral gradual change from nonrecrystallized to a partially or completely recrystallized zone with observable transitional stages, and 2) the presence of relics of the initial acicular aragonite encased in secondary ray aragonite crystals (Fig. 11C). Such recrystallization is expressed only through textural change (i.e., modification of the size and geometry of individual crystals) and no change in mineralogy. In addition, no marked differences in Sr content between the primary and secondary aragonite is evident on the backscattered SEM images or with the EDS and WDS microprobes (Table 2).

Similar isomineral recrystallization of biogenic carbonates have already been described in the marine realm, resulting from textural changes of biogenic aragonites in corals (Repellin 1977; Perrin 2004) and in the green algae *Halimeda* (Macintyre and Reid 1995) or modifications of skeletal Mg calcite in the foraminifer *Archaias* (Macintyre and Reid 1998; Reid and Macintyre 1998; Hover et al. 2001). In *Halimeda* and *Archaias*, the process of isomineralogical recrystallization has been shown to take place in living organisms or at very early post-mortem stage. In coral skeletons, the skeletal aragonite fiber, initially formed of numerous submicrometer-size elementary biocrystals in optical continuity, is recrystallized gradually into a unique aragonite crystal; adjacent fibers can also merge together during this process (Perrin 2004). The recrystallization of submicrometer-size crystals into larger crystals (Ostwald ripening) minimizes the surface free energy of crystals and is therefore driven by thermodynamical constraints. A similar Ostwald ripening process can explain the isomineralogical recrystallization of aragonite in speleothems (Fig. 11B, C), although in corals, initiation of the process is further favored by hydrolysis and breakup of organic skeletal matrices (Perrin and Smith 2007a).

Aragonite–Calcite.—The recrystallization process is a wet transformation, taking place across thin water film 100 Å to 1 µm in thickness, which

forms an interface with dissolution of aragonite initiating on one side and precipitation of calcite occurring at the same time on the other side (Kinsman 1969; Pingitore 1976; Brand and Veizer 1980). This process requires that diagenetic waters be undersaturated with respect to aragonite and oversaturated with respect to calcite, although the presence of some cations, most commonly Mg, can influence the degree of supersaturation and, hence, favor precipitation of aragonite over calcite (Choudens-Sánchez and González 2009). For the pseudomorphic replacement of one polymorph by the other, the two processes, dissolution and precipitation, must be coupled at the interface formed by the thin water film with identical dissolution and precipitation rates. The reaction proceeds through the migration of this interface (i.e., the thin water film), implying fluid transport pathways at the recrystallization front (Perdikouri et al. 2008). Very locally, the precipitation of calcite can generate supersaturation with respect to aragonite, leaving undissolved aragonite crystals as relics in the diagenetic calcite. Although the aragonite-calcite recrystallization does not imply changes in major element (i.e., Ca, C, O) content, a general depletion of Sr associated with an enrichment in Mg in the recrystallized final product has been reported by many workers in both continental and marine carbonates (e.g., Kinsman 1969; Pingitore 1976; Brand and Veizer 1980), including speleothems (e.g., Frisia et al. 2002; Perdikouri et al. 2008; Martin-Perez et al. 2012). In contrast to common interpretations, the neomorphic calcite does not inherit the geochemical (including isotopic) signature of its aragonite precursor (e.g., Frisia et al. 2002, for the U content and carbon isotope value in calcite of recrystallization). Instead, this apparent inheritance is simply due to the presence of aragonite relics. Hence, the resulting geochemical signal is an intermediate value between the signal of aragonite and the signal of recrystallization calcite, because the measured sample is a mixture of primary aragonite and secondary calcite crystals. Thus, the value varies with the sampling size, depending on the ratio of calcite to aragonite in the analysis (Fig. 16). P-XRF measures on slab specimens of stalactites and stalagmites from the Pont-de-Ratz Cave show Sr values between 450 and 650 ppm, in zones where recrystallization of aragonite into sparry calcite occurred (Fig. 16). These Sr values clearly are lower than the Sr content of the primary aragonite but much higher than what would be expected from a pure calcite. In fact, sparry calcites in the same and in other similar zones include an Sr content below the detection limit of the microprobe (i.e., < 450 ppm). The Sr content of these recrystallized areas obviously is included in the aragonite relics. Therefore, the use of analytical techniques permitting a visual control of the position of the analytical spot, together with the spatial resolution of this area, appears of tremendous importance in diagenetic studies of

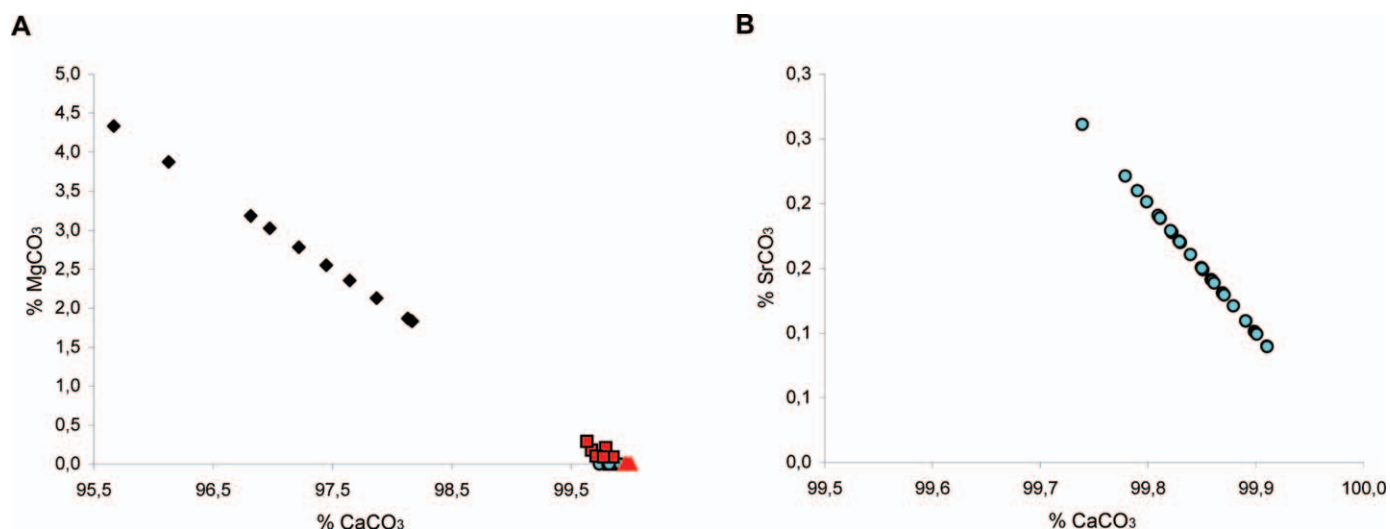


Fig. 17.—Impact of aragonite–calcite recrystallization on the geochemistry of spelean carbonates (measures WDS microprobe, detection limits provided in text “Methods and Material”). **A)** Variation of % MgCO₃ from primary aragonite, with no detectable Mg (blue dots) to ending products of the two aragonite–calcite recrystallizations: columnar calcite (black diamonds) and sparry calcite with detectable Mg content (red squares) and non-detectable Mg on crystal margins (red triangles). **B)** % SrCO₃ in primary aragonite (non-detectable Mg).

spelean carbonates. In the particular case of Mg and Sr, the combined effect of Mg enrichment and Sr depletion during the aragonite-to-calcite recrystallization is governed by the respective geometrical constraints of the aragonite and calcite crystal lattices defining the nature of crystallographic site of the trace element: the orthorhombic aragonite lattice, in which cations are in nine-fold coordination with carbonate oxygens, accepts cations with a ionic radius slightly higher than the Ca²⁺ diameter in substitution for calcium (e.g., Sr²⁺, Ba²⁺) while the rhombohedral calcite lattice, in which cations are in six-fold coordination with carbonate oxygens, is readily capable of incorporating cations with a ionic radius slightly smaller than the Ca²⁺ diameter in substitution for calcium (e.g., Mg²⁺). As underlined by Morse et al. (2007, p. 345), “these coprecipitation trends are best qualitative statements and observed distributions have shown poor fidelity with attempts to define partitioning on purely thermodynamic grounds.” Finally, Sr/Ca and Mg/Ca ratios in natural carbonate minerals are driven by interaction between the differential coordination of Sr and Mg in calcite and aragonite (Finch and Allison 2007) and the efficacy of aqueous diffusion during diagenesis (Pingitore 1982). The aragonite–calcite recrystallization consequently is an open-system reaction during which dissolution of aragonite tends to liberate Sr²⁺ cations in the solution and the concomitant crystallization of calcite tends to take, up to a certain point, Mg²⁺ ions from the diagenetic fluid, which are incorporated in the crystal lattice.

Two distinct types of aragonite–calcite recrystallization occur in the stalagmites of the Pont-de-Ratz Cave. The distinction between these two types of recrystallization is based on the clear difference between ending products: sparry calcite and columnar calcite, both of which differ in the crystals morphology (Figs. 11, 13) and chemistry (Mg content) (Table 2). There is no intermediate form, or gradation, between these two different calcites. The implications of such differences in terms of diagenetic pathways and possible scenarios for these recrystallization processes in relation to properties of drip water are proposed and discussed below.

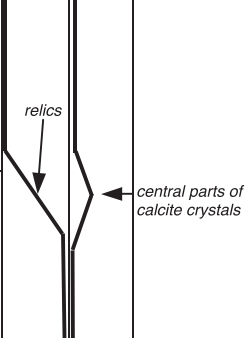
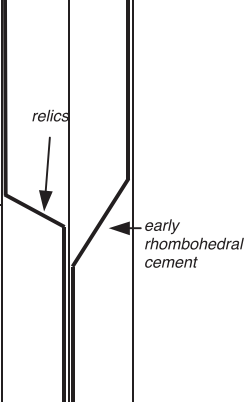
Aragonite–Sparry Calcite Recrystallization has been described in several works, including speleothem studies. Frisia (1996) described a slightly different type of recrystallization, a mimetic transformation of aragonite rays into mosaic sparry calcite, which has not been observed in the specimens from the Pont-de-Ratz Cave. In these samples, aragonite–sparry calcite recrystallization occurs through transformation

of aragonite into polygon-like crystals of non-Mg sparry calcite (Table 2) containing numerous relics of the aragonite precursor (Fig. 11D–F). Microprobe analyses show that the Mg content of calcite tends to decrease towards the periphery of the sparry crystal, and hence include a marked decrease of Mg incorporated in the calcite lattice in the course of the reaction (Fig. 12A, B). In other words, the pore-fluid composition evolves in the course of the recrystallization process. This evolution of pore-fluid composition is induced by calcite precipitation, which consumes some Mg available in the pore fluid for incorporation in the crystal lattice. The early calcite phases hence have slightly higher Mg content and the total amount of Mg, which can be removed from solution for incorporation in the calcite crystals before growth of the entire crystal (Fig. 12B). This interpretation suggests that the recharge of diagenetic water is not efficient to prevent the Mg/Ca ratio to decrease in the course of the recrystallization process, even though the amount of Mg²⁺ ions incorporated into the calcite lattice remains low. In other words, the recharge rate of diagenetic water is slow compared to the recrystallization rate.

These results show that this type of recrystallization on the geochemical composition of the original precipitates leads to a loss of Sr (and, hence, a decrease in the Sr/Ca ratio). This loss is accompanied by a slight but temporary increase in the Mg/Ca ratio during the first steps of the recrystallization, followed by a decrease in Mg towards final stage of the process (Fig. 17A, B).

Aragonite–Columnar Calcite Recrystallization leads to transformation of aragonite into elongate crystals of low-Mg columnar calcite (Fig. 13A, B), with a morphology similar to that of the primary columnar calcite precipitated directly from drip water. The recrystallization process is demonstrated petrographically by aragonite passing to columnar calcite in the same growth layer (because each individual lamina precipitated with the same mineralogy; Fig. 13B, C) or relic crystals of aragonite precursor included in columnar calcite crystals (Fig. 13D). The aragonite–columnar calcite recrystallization starts with precipitation of rhombohedral calcite crystals cementing the surfaces of ray aragonite crystals (Figs. 5F, 15A–C). Further growth of calcite rhombohedrons associated with spatial competition between individual crystals tends to gradually increase the crystal size (Fig. 15C) and homogenize crystal orientation. The dissolution–precipitation process gradually takes over

TABLE 5.—Various types of temporal changes from aragonite to calcite in speleothems, their impact on carbonate geochemistry and on the preservation of the paleoenvironmental signal.

Nature of change and process	Characteristic features	Temporal significance of spatial distribution	Type of products	Impact on carbonate geochemistry			Potential use for paleoenvironmental studies	
				Sr - +	Mg - +		preservation of paleoclimatic signal	potential for dating
Change in the mineralogy of precipitates during stalagmite growth	<ul style="list-style-type: none"> - spatial distribution of precipitates in "stratigraphical" succession - abrupt contact between both carbonate phases - growth discontinuity resulting from change of mineralogy 	correlation between spatial and temporal distribution	Primary columnar calcite cement				<ul style="list-style-type: none"> - High potential for preservation of signal - Preservation of laminae if any 	U/Th dating possible for both primary aragonite and calcite
			Primary aragonite			<i>discontinuity</i>		
Recrystallization of aragonite into sparry calcite	<ul style="list-style-type: none"> - no discontinuity surface at contact between both minerals - gradation between non-recrystallized and completely recrystallized zones - frequent aragonite relics in calcite crystals 	spatial distribution does not reflect time gradient	Recrystallization sparry calcite				<ul style="list-style-type: none"> - Signal not preserved in totally recrystallized zones and significantly altered in partially recrystallized zones - laminae completed or strongly altered 	No dating possible due to system reopening during recrystallization processes
			Primary aragonite					
Recrystallization of aragonite into columnar calcite	<ul style="list-style-type: none"> - no discontinuity surface at contact between both minerals - gradation between non-recrystallized and completely recrystallized zones - scarce aragonite relics in calcite crystals - lateral mineralogical shift in same layer 	spatial distribution does not reflect time gradient	Recrystallization columnar calcite				<ul style="list-style-type: none"> - Signal not preserved in totally recrystallized zones and significantly altered in partially recrystallized zones - Laminae completed or strongly altered 	No dating possible due to system reopening during recrystallization processes
			Primary aragonite					

from this earliest cementation phase, leading to the development of much larger crystals of columnar calcite (Fig. 15D). Frisia et al. (2002) have observed comparable calcite cement developed between aragonite crystals at the tips of aragonite stalagmites in the Clamouse Cave (southern France). These authors suggest that such calcite cement could have promoted recrystallization of aragonite by acting as preferential sites for calcite nucleation and consider this as an early step of the recrystallization process, although in this case, a simple aragonite-to-calcite succession of precipitates from drip water without recrystallization could alternatively explain the described observations. However, that aragonite–calcite recrystallization clearly differs from the recrystallization of aragonite into columnar calcite described here (Fig. 15), appearing more akin to the recrystallization of aragonite into sparry calcite. Similarly, Martin-Perez et al. (2012) described a two-step process

of aragonite–calcite transformation in a drapery speleothem from Castañar del Ibor Cave in Spain, leading to recrystallization of aragonite into an equant mosaic of calcite crystals (i.e., sparite). In the Pont-de-Ratz samples, element analyses show that the Mg content is the same in the early small calcite rhombohedrons and in the secondary columnar calcite, indicating that the Mg/Ca ratio of the diagenetic fluid remains the same in the course of the recrystallization process (Table 2). Since the aragonite precursor does not contain detectable Mg, recrystallization of aragonite to columnar calcite necessarily takes place in waters with a sufficient Mg/Ca ratio to result in the present Mg content. Moreover, the maintenance of a constant Mg/Ca ratio during the recrystallization process may require persistent recharge of diagenetic fluids. In this case, the recharge rate of diagenetic water is high compared to the recrystallization rate.

Analyses of the Pont-de-Ratz material demonstrate that alteration of the initial geochemical properties of the carbonate material in relation to this type of recrystallization results in a decrease of the Sr/Ca ratio, associated with a marked increase in the Mg/Ca ratio (Fig. 17A, B). Therefore, the two aragonite–calcite recrystallizations impact the geochemistry of the initial precursor differently (Fig. 17A, Table 5).

Furthermore, results show that three different types of aragonite-to-calcite evolution through time can occur in cave settings, through distinct depositional or postdepositional processes (i.e., mineralogical shift in carbonate precipitation from drip water, and the two recrystallizations) each with the distinct criteria for recognition (Table 5). Their impact on the geochemical properties of carbonate phases, their significance in term of speleothem history, and finally their effect on the preservation of paleoclimatic (e.g., geochemical and other proxies such as lamination) and geochronological signals are extremely different and represent important issues for the reliability of further paleoenvironmental research (Table 5).

The Origin of Columnar Calcite has led to strong debates during the past decade (Gonzalez et al. 1992, 1993; Kendall 1993; Frisia et al. 2000). The results of Railsback et al. (2002), which demonstrated the occurrence of secondary columnar calcite produced by recrystallization in speleothems of the Wadi Sannur Cavern in Egypt, suggest that recrystallization leading to secondary columnar calcite may be common. Therefore, the primary *versus* secondary nature of columnar calcites is an important issue in speleothem research, and clear criteria for discriminating primary and recrystallized calcite are needed (Figs. 10, 13). The results of this study show that in speleothems of the Pont-de-Ratz Cave, a slightly higher Mg concentration occurs in recrystallized columnar calcites than in primary columnar calcites, although two ranges overlap (Table 2). As a result, petrology, especially the observation of the presence of precursor relics (Fig. 13D), is the most reliable tool for unambiguously distinguishing the types of calcite.

CONCLUSIONS

Coupled petrographical, geochemical, and mineralogical study of speleothems from the Pont-de-Ratz Cave provides the following results:

- Growth of stalagmites was driven alternatively by precipitation of two distinct aragonites and a columnar calcite.
- Speleothem growth was disturbed or interrupted periodically, as suggested by growth discontinuities and inclusions levels which potentially record environmental events at different spatial scales.
- Speleothem precipitates are affected by textural, geochemical, and mineralogical modifications depending on physicochemical variations of microenvironmental parameters during diagenetic history. The initial carbonate materials are therefore evolving through time.
- Speleothem diagenetic processes take place below the stalagmite external surface. These dynamics require migration of water through microporosity by capillarity towards the diagenetic sites. The processes include cementation, dissolution, and recrystallization of extant speleothem material.
- Three different types of recrystallization are evident: early aragonite–aragonite recrystallization, and two distinct aragonite–calcite (aragonite–sparry calcite and aragonite–columnar calcite) recrystallizations. The two aragonite–calcite recrystallizations produce secondary calcite which differs in crystal morphology, texture, and Mg content, indicating slight but distinct differences in the Mg/Ca ratio of the diagenetic water and in the balance between diagenetic fluid recharge rate and recrystallization rate.
- Columnar calcites can either be directly precipitated (primary speleothem growth) or occur as a recrystallization product of precursor aragonite. The primary and secondary columnar calcites

from the Pont-de-Ratz Cave can be unequivocally identified from petrography.

These results highlight the importance of diagenesis in the geochemical archives of vadose speleothems, and the large variety of potential syngenetic and postformational modifications of speleothem precipitates in cave environments. Furthermore, this work emphasizes the value of coupled petrography and geochemical study for identifying the nature and origin of the diverse speleothem materials and their postdepositional modification. Moreover, the results provide criteria for recognition of growth history and diagenetic history to be clearly discriminated, and criteria for assessment of the impact of diagenetic processes on the original geochemistry of these carbonates, and hence on the preservation of environmental signals in speleothem material. Such an integrated analytical approach allows judicious selection of speleothem material favorable for radiometric dating and extraction of reliable paleoenvironmental proxies.

ACKNOWLEDGMENTS

We are particularly grateful to the two speleology clubs of the Saint-Pons and the city of Saint-Pons-de-Thomières, which facilitate access to the cave. Technical preparation of samples is especially thanked: Michel Lemoine and Lilian Caze (CR2P, MNHN, Paris) for thin-section and sample preparation, Jean-François Mena (LMTG, University of Toulouse) for preparation of SEM and microprobe specimens. We sincerely thank also technical assistance nicely provided by Thierry Aigouy (SEM and EDS, LMTG), Sylvain Pont (SEM and EDS, MNHN), Philippe de Parseval (WDS, LMTG), and Gilles Montagnac (Raman microspectrometry, ENS Lyon). Aquila-Conseil is warmly acknowledged for lending the P-XRF spectrometer. Bruce Railsback, an anonymous reviewer, and JSR Associate Editor Leslie Melim are sincerely thanked for their useful comments on the manuscript.

REFERENCES

- AISSAOUI, D.M., 1985, Botryoidal aragonite and its diagenesis: *Sedimentology*, v. 32, p. 345–361.
- AISSAOUI, D.M., 1988, Magnesian calcite cements and their diagenesis: dissolution and dolomitization, Mururoa Atoll: *Sedimentology*, v. 35, p. 821–841.
- AISSAOUI, D.M., BUIGUES, D., AND PURSER, B.H., 1986, Model of reef diagenesis: Mururoa Atoll, French Polynesia, in Schroeder, J.H., and Purser, B.H., eds., *Reef Diagenesis*: Berlin, Springer-Verlag, p. 27–52.
- ALABOUVETTE, B., DEMANGE, M., DE SAUVAL, C., AND AUTRELLE, C., 1993, Notice explicative, Carte géologique France (1/50 000), feuille Saint-Pons (1013), BRGM, Orléans, 123 p.
- ASMERON, Y., POLYAK, V., BURNS, S., AND RASMUSSEN, J., 2007, Solar forcing of Holocene climate: new insights from a speleothem record, southwestern United States: *Geology*, v. 35, p. 1–4.
- ASMERON, Y., POLYAK, V., AND BURNS, S., 2010, Variable winter moisture in the southwestern United States linked to rapid glacial climate shifts: *Nature Geoscience*, v. 3, p. 114–117.
- AUDRA, P., HOBLEA, F., BIGOT, J.-Y., AND NOBECOURT, J.-C., 2007, The role of condensation-corrosion in thermal speleogenesis: study of a hypogenic sulfidic cave in Aix-les-Bains, France: *Acta Carsologica*, v. 36, p. 185–194.
- AULER, A.S., AND SMART, P.L., 2004, Rates of condensation corrosion in speleothems of semi-arid northeastern Brazil: *Speleogenesis and Evolution of Karst Aquifers*, v. 2, p. 1–2.
- BADIOZAMANI, K., MACKENZIE, F.T., AND THORSTENSON, D.C., 1977, Experimental carbonate cementation: salinity, temperature and vadose–phreatic effects: *Journal of Sedimentary Petrology*, v. 47, p. 529–542.
- BATHURST, R.G.C., 1971, *Carbonate Sediments and Their Diagenesis*: Amsterdam, Elsevier, 620 p.
- BERTHAUX, J., SONDAG, F., SANTOS, R., SOUBIÈS, F., CAUSSE, C., PLAGNES, V., LE CORNEC F., AND SEIDEL, A., 2002, Paleoclimatic record of speleothems in a tropical region: study of laminated sequences from a Holocene stalagmite: *Quaternary International*, v. 89, p. 3–16.
- BRAND, U., AND ZEISER, J., 1980, Chemical diagenesis of a multicomponent carbonate system, 1: trace elements: *Journal of Sedimentary Petrology*, v. 50, p. 1219–1236.
- BUHMANN, D., AND DREYBRODT, W., 1985a, The kinetics of calcite dissolution and precipitation in geologically relevant situations of karst areas 1. Open system: *Chemical Geology*, v. 48, p. 189–211.
- BUHMANN, D., AND DREYBRODT, W., 1985b, The kinetics of calcite dissolution and precipitation in geologically relevant situations of karst areas 2. Closed system: *Chemical Geology*, v. 53, p. 109–124.

- CABROL, P., 1978, Contribution à l'étude du concrétionnement carbonaté des grottes du Sud de la France, morphologie, genèse, diagenèse: Mémoires du Centre d'Etudes et de Recherches Géologiques et Hydrogéologiques, v. 12, Montpellier, 275 p.
- CABROL, P., AND COUDRAY, J., 1982, Climatic fluctuations influence in the genesis and diagenesis of carbonate speleothems in southwestern France: National Speleological Society, Bulletin, v. 44, p. 112–117.
- CADDEO, G.A., DE WAELE, J., FRAU, F., AND RAILSBACK, L.B., 2011, Trace element and stable isotope data from a flowstone in a natural cave of the mining district of SW Sardinia (Italy): evidence for Zn^{2+} -induced aragonite precipitation in comparatively wet climatic conditions: International Journal of Speleology, v. 40, p. 181–190.
- CHENG, H., EDWARDS, R.L., BROECKER, W.S., DENTON, G.H., KONG, X., WANG, Y., ZHANG, R., AND WANG, X., 2009, Ice age terminations: Science, v. 326, p. 248–252.
- DE CHOUDENS-SÁNCHEZ, V., AND GONZÁLEZ, L.A., 2009, Calcite and aragonite precipitation under controlled instantaneous supersaturation: elucidating the role of $CaCO_3$ saturation state and Mg/Ca ratio on calcium carbonate polymorphism: Journal of Sedimentary Research, v. 79, p. 363–376.
- DE FREITAS, C.R., AND SCHMEKAL, A.A., 2006, Studies of condensation/evaporation processes in the Glowworm Cave, New Zealand: International Journal of Speleology, v. 35, p. 75–81.
- DELHAYE, M., AND DHAMELINCOURT, P., 1975, Raman microprobe and microscope with laser excitation: Journal of Raman Spectroscopy, v. 3, p. 33.
- DHAMELINCOURT, P., AND BISSON, P., 1977, Principe et réalisation d'un microscope optique utilisant l'effet Raman: Microscopica Acta, v. 79, p. 267–276.
- DICKSON, J.A.D., 1983, Graphical modelling of crystal aggregates and its relevance to cement diagenesis: Royal Society of London, Philosophical Transactions, v. A 309, p. 465–502.
- DICKSON, J.A.D., 1993, Crystal growth diagrams as an aid to interpreting the fabrics of calcite aggregates: Journal of Sedimentary Petrology, v. 63, p. 1–18.
- DREDGE, J., FAIRCHILD, I.J., HARRISON, R.M., FERNÁNDEZ-CORTES, A., SÁNCHEZ-MORAL, S., JURADO, V., GUNN, J., SMITH, A., SPÖTL, C., MATTEY, D., WYNN, P.M., AND GRASSINEAU, N., 2013, Cave aerosols: distribution and contribution to speleothem geochemistry: Quaternary Science Reviews, v. 63, p. 23–41.
- DREYBRODT, W., LAUCKNER, J., ZAIHUA, L., SVENSSON, U., AND BUHMANN, D., 1996, The kinetics of the reaction $CO_2 + H_2O \rightarrow H^+ + HCO_3^-$ as one of the rate limiting steps for the dissolution of calcite in the system $H_2O-CO_2-CaCO_3$: Geochimica et Cosmochimica Acta, v. 60, p. 3375–3381.
- DREYBRODT, W., EISENLOHR, L., MADRY, B., AND RINGER, S., 1997, Precipitation kinetics of calcite in the system $CaCO_3-H_2O-CO_2$: the conversion to CO_2 by the slow process $H^+ + HCO_3^- \rightarrow CO_2 + H_2O$ as a rate limiting step: Geochimica et Cosmochimica Acta, v. 61, p. 3897–3904.
- DREYBRODT, W., GABROVEK, F., AND PERNE, M., 2005, Condensation corrosion: a theoretical approach: Acta Carologica, v. 34, p. 317–348.
- DRYSDALE, R.N., HELLSTROM, J.C., ZANCHETTA, G., FALICK, A.E., SÁNCHEZ GON, M.F., COUCHOUD, I., McDONALD, J., MAAS, R., LOHMANN, G., AND ISOLA, I., 2009, Evidence for obliquity forcing of glacial termination II: Science, v. 325, p. 1527–1531.
- DUBLYANSKY, V.N., AND DUBLYANSKY, Y.V., 1998, The problem of condensation in karst studies: Journal of Cave and Karst Studies, v. 60, p. 3–17.
- DULLO, W.C., 1986, Variation in diagenetic sequences, an example from Pleistocene coral reefs, Red Sea, Saudi Arabia, in Schroeder, J.H., and Purser, B.H., eds., Reef Diagenesis: Berlin, Springer-Verlag, p. 77–90.
- FAIRCHILD, I.J., AND BAKER, A., 2012, Speleothem Science: From Process to Past Environment: Chichester, Wiley-Blackwell, 450 p.
- FAIRCHILD, I.J., FRISIA, S., BORSATO, A., AND TOOTH, A.F., 2006a, Speleothems, in Nash, D.J., and McLaren, S.J., eds., Geochemical Sediments and Landscapes: Oxford, U.K., Blackwell, p. 1–21.
- FAIRCHILD, I.J., SMITH, C.L., BAKER, A., FULLER, L., SPÖTL, C., MATTEY, D., AND McDERMOTT, F., 2006b, Modification and preservation of environmental signals in speleothems: Earth-Science Reviews, v. 75, p. 105–153.
- FERNÁNDEZ-DÍAZ L., PUTNIS, A., PRIETO, M., AND PUTNIS, C.V., 1996, The role of magnesium in the crystallization of calcite and aragonite in a porous medium: Journal of Sedimentary Research, v. 66, p. 482–491.
- FINCH, A.A., AND ALLISON, N., 2007, Coordination of Sr and Mg in calcite and aragonite: Mineralogical Magazine, v. 71, p. 539–552.
- FINCH A.A., SHAW, P.A., WEEDON, G.P., AND HOLMGREN, K., 2001, Trace element variation in speleothem aragonite: potential for palaeoenvironmental reconstruction: Earth and Planetary Science Letters, v. 186, p. 255–267.
- FINCH, A.A., SHAW, P.A., HOLMGREN, K., AND LEE-THORP, J., 2003, Corroborated rainfall records from aragonite stalagmites: Earth and Planetary Science Letters, v. 215, p. 265–273.
- FISCHBECK, R., AND MÜLLER, G., 1971, Monohydrocalcite, hydromagnesite, nesquehite, dolomite, aragonite, and calcite in speleothems of the Fränkische Schweiz, Western Germany: Contributions to Mineralogy and Petrology, v. 33, p. 87–92.
- FLÜGEL, E., 2010, Microfacies of Carbonate Rocks: Analysis, Interpretation and Application: Berlin, Springer-Verlag, 984 p.
- FOLK, R.L., 1965, Some aspects of recrystallization in ancient limestones, in Pray, L.C., and Murray, R.C., eds., Dolomitization and Limestone Diagenesis: SEPM, Special Publication 13, p. 14–48.
- FOLK, R.L., AND ASSERETO, R., 1976, Comparative fabrics of length-slow and length-fast calcite and calcitized aragonite in a Holocene speleothem, Carlsbad Caverns, New Mexico: Journal of Sedimentary Petrology, v. 46, p. 486–496.
- FORD, D.C., AND WILLIAMS, P., 2007, Karst Hydrogeology and Geomorphology, Second Edition: Chichester, John Wiley & Sons, 562 p.
- FRISIA, S., 1996, Petrographic evidences of diagenesis in speleothems: some examples: Speleochronos, v. 7, p. 21–30.
- FRISIA, S., AND BORSATO, A., 2010, Karst, in Alonso-Zarza, A.M., and Tanner, L.H., eds., Carbonates in Continental Settings: Amsterdam, Elsevier, Developments in Sedimentology 61, p. 269–318.
- FRISIA, S., BORSATO, A., FAIRCHILD, I.J., AND McDERMOTT, F., 2000, Calcite fabrics, growth mechanisms, and environments of formation in speleothems from the Italian Alps and southwestern Ireland: Journal of Sedimentary Research, v. 70, p. 1183–1196.
- FRISIA, S., BORSATO, A., FAIRCHILD, I.J., McDERMOTT, F., AND SELMO, E.M., 2002, Aragonite-calcite relationships in speleothems (Grotte de Clamouse, France): environment, fabrics, and carbonate geochemistry: Journal of Sedimentary Research, v. 72, p. 687–699.
- GINSBURG, R.N., MARZALEK, D.S., AND SCHNEIDERMAN, N., 1971, Ultrastructure of carbonate cements in a Holocene algal reef of Bermuda: Journal of Sedimentary Petrology, v. 41, p. 472–482.
- GONZÁLEZ, L.A., CARPENTER, S.J., AND LOHMANN, K.C., 1992, Inorganic calcite morphology: roles of fluid chemistry and fluid flow: Journal of Sedimentary Petrology, v. 62, p. 382–399.
- GONZÁLEZ, L.A., CARPENTER, S.J., AND LOHMANN, K.C., 1993, Columnar calcite in speleothems: Reply: Journal of Sedimentary Petrology, v. 63, p. 553–556.
- GVIRTZMAN, G., AND FRIEDMAN, G.M., 1977, Sequence of progressive diagenesis in coral reefs, in Frost, S.H., Weiss, M.P., and Saunders, J.B., eds., Reefs and Related Carbonates, Ecology and Sedimentology: American Association of Petroleum Geologists, Studies in Geology 4, p. 357–380.
- HARMON, R.S., ATKINSON, T.C., AND ATKINSON, J.L., 1983, The mineralogy of Castleguard Cave, Columbia Icefields, Alberta Canada: Arctic and Alpine Research, v. 15, p. 503–516.
- HARRIS, P.M., KENDALL, C.G.St.C., AND LERCHE, I., 1985, Carbonate cementation: a brief review, in Schneidermann, N., and Harris, P.M., eds., Carbonate Cements: SEPM, Special Publication 36, p. 79–95.
- HARTLAND, H., FAIRCHILD, I.J., LEAD, J.R., BORSATO, A., BAKER, A., FRISIA, S., AND BAALOUSHA, M., 2012, From soil to cave: transport of trace metals by natural organic matter in cave dripwaters: Chemical Geology, v. 304–305, p. 68–82.
- HOPLEY, P.J., MARSHALL, J.D., AND LATHAM, A.G., 2009, Speleothem preservation and diagenesis in South African Hominin sites: implications for palaeoenvironments and geochronology: Geoarchaeology, v. 24, p. 519–547.
- HOVER, V.C., WALTER, L.M., AND PEACOR, D.R., 2001, Early marine diagenesis of biogenic and Mg-calcite: new constraints from high-resolution STEM and AEM analyses of modern platform carbonates: Chemical Geology, v. 175, p. 221–248.
- JAMES, N.P., 1974, Diagenesis of scleractinian corals in the subaerial vadose environment: Journal of Paleontology, v. 48, p. 785–799.
- JONES, B., 2009, Cave pearls: the integrated product of abiogenic and biogenic processes: Journal of Sedimentary Research, v. 79, p. 689–710.
- KENDALL, A.C., 1993, Columnar calcite in speleothems: Discussion: Journal of Sedimentary Petrology, v. 63, p. 550–552.
- KENDALL, A.C., AND BROUGHTON, P.L., 1978, Origin of fabrics in speleothems composed of columnar calcite crystals: Journal of Sedimentary Petrology, v. 48, p. 519–538.
- KINSMAN, D.J.J., 1969, Interpretation of Sr^{2+} concentrations in carbonate minerals and rocks: Journal of Sedimentary Petrology, v. 39, p. 486–508.
- LACHNIET, M.S., 2009, Climatic and environmental controls on speleothem oxygen-isotope values: Quaternary Science Reviews, v. 28, p. 412–432.
- LAURITZEN, S.E., AND LUNDBERG, J., 1999, Speleothems and climate: The Holocene, v. 9, p. 643–647.
- MACHEL, H.G., 1997, Recrystallization versus neomorphism, and the concept of “significant recrystallization” in dolomite research: Sedimentary Geology, v. 113, p. 161–168.
- MACINTYRE, I.G., 1977, Distribution of submarine cements in a modern Caribbean fringing reef, Galeta Point, Panama: Journal of Sedimentary Petrology, v. 47, p. 503–516.
- MACINTYRE, I.G., AND REID, R.P., 1995, Crystal alteration in a living calcareous alga (*Halimeda*): implications for studies in skeletal diagenesis: Journal of Sedimentary Research, v. 65, p. 143–153.
- MACINTYRE, I.G., AND REID, R.P., 1998, Recrystallization in living porcelaneous foraminifera (*Archais angulatis*): textural changes without mineralogical alteration: Journal of Sedimentary Research, v. 68, p. 11–19.
- MARTÍN-GARCÍA, R., ALONSO-ZARZA, A.M., AND MARTÍN-PÉREZ, A., 2009, Loss of primary texture and geochemical signatures in speleothems due to diagenesis: evidences from Castañar Cave, Spain: Sedimentary Geology, v. 221, p. 141–149.
- MARTÍN-PÉREZ, A., MARTÍN-GARCÍA, R., AND ALONSO-ZARZA, A.M., 2012, Diagenesis of a drapery speleothem from Castañar Cave: from dissolution to dolomitization: International Journal of Speleology, v. 41, p. 251–266.
- MAZZULLO, S.J., 1980, Calcite pseudospin replacement of marine acicular aragonite and implications for aragonite cement diagenesis: Journal of Sedimentary Petrology, v. 50, p. 409–422.
- McMILLAN, E.A., FAIRCHILD, I.J., FRISIA, S., BORSATO, A., AND McDERMOTT, F., 2005, Annual trace element cycles in calcite-aragonite speleothems: evidence of drought in the western Mediterranean 1200–1100 yr BP: Journal of Quaternary Science, v. 20, p. 423–433.
- MELIM, L.A., AND SPILDE, M.N., 2011, Rapid growth and recrystallization of cave pearls in an underground limestone mine: Journal of Sedimentary Research, v. 81, p. 775–786.

- MEYER, M.C., CLIFF, R.A., SPÖTL, C., KNIPPING, M., AND MANGINI, A., 2009, Speleothems from the earliest Quaternary: snapshots of paleoclimate and landscape evolution at the northern rim of the Alps: *Quaternary Science Reviews*, v. 26, p. 1374–1391.
- MEYER, M.C., LIFF, R.A., AND SPÖTL, C., 2011, Speleothems and mountain uplift: *Geology*, v. 39, p. 447–450.
- MORSE, J.W., AND MACKENZIE, F.T., 1990, *Geochemistry of Sedimentary Carbonates*: Amsterdam, Elsevier, 707 p.
- MORSE, J.W., ARVIDSON, R.S., AND LÜTTGE, A., 2007, Calcium carbonate formation and dissolution: *Chemical Review*, v. 107, p. 342–381.
- ONAC, B.P., AND FORTI, P., 2011, Minerogenetic mechanisms occurring in the cave environment: an overview: *International Journal of Speleology*, v. 40, p. 79–98.
- NASDALA, L., SMITH, D.C., KAINDL, R., GAFT, M., AND ZIEMANN, M.A., 2004, Raman spectroscopy: Analytical perspectives in mineralogical research, in Beran, A., and Libowitzky, E., eds., *Spectroscopic Methods in Mineralogy*: Budapest, Eotvos University Press, EMU Notes in Mineralogy 6, p. 281–343.
- PERDIKOURI, C., KASIOPTAS, A., PUTNIS, C.V., AND PUTNIS, A., 2008, The effect of fluid composition on the mechanism of the aragonite to calcite transition: *Mineralogical Magazine*, v. 72, p. 111–114.
- PERRIN, C., 2003, Compositional heterogeneity and microstructural diversity of coral skeletons: implications for taxonomy and control on early diagenesis: *Coral Reefs*, v. 22, p. 109–120.
- PERRIN, C., 2004, Diagenèse précoce des biocristaux carbonatés: transformations isomériques de l'aragonite corallienne: *Société Géologique de France, Bulletin*, v. 175, p. 95–106.
- PERRIN, C., 2010, Diagenesis, in Hopley, D., ed., *Encyclopedia of Modern Coral reefs*: Berlin, Springer-Verlag, p. 309–321.
- PERRIN, C., AND CUIF, J.P., 2001, Ultrastructural controls on diagenetic patterns of scleractinian skeletons: evidence at the scale of colony life-time: *Tohoku University Museum, Bulletin*, v. 1, p. 210–218.
- PERRIN, C., AND SMITH, D.C., 2007a, Decay of organic skeletal matrices as control on early diagenesis of coral skeletons: *Comptes Rendus Palevol*, v. 6, p. 253–260.
- PERRIN, C., AND SMITH, D.C., 2007b, Earliest steps of diagenesis in living coral skeletons: evidence from ultrastructural pattern and Raman spectroscopy: *Journal of Sedimentary Research*, v. 77, p. 495–507.
- PINGITORE, N.E., 1976, Vadose and phreatic diagenesis: processes, products, and their recognition in corals: *Journal of Sedimentary Petrology*, v. 46, p. 985–1006.
- PINGITORE, N.E., 1978, The behavior of Zn^{2+} and Mn^{2+} during carbonate diagenesis: theory and applications: *Journal of Sedimentary Petrology*, v. 48, p. 799–814.
- PINGITORE, N.E., 1982, The role of diffusion during carbonate diagenesis: *Journal of Sedimentary Petrology*, v. 52, p. 27–39.
- POKROVSKY, O.S., GOLUBEV, S.V., AND SCHOTT, J., 2005, Dissolution kinetics of calcite, dolomite and magnesite at 25°C and 1 to 50 atm pCO_2 : *Chemical Geology*, v. 217, p. 239–255.
- PURDY, E.G., 1968, Carbonate diagenesis: an environmental survey: *Geologica Romana*, v. 7, p. 183–228.
- RAILSBACK, L.B., BROOK, G.A., CHEN, J., KALIN, R., AND FLEISHER, C.J., 1994, Environmental controls on the petrology of a late Holocene speleothem from Botswana with annual layers of aragonite and calcite: *Journal of Sedimentary Research*, v. 64, p. 147–155.
- RAILSBACK, L.B., DABOUS, A.A., OSMOND, J.K., AND FLEISHER, C.J., 2002, Petrographic and geochemical screening of speleothems for U-series dating: an example from recrystallized speleothems from Wadi Sannur Cavern, Egypt: *Journal of Cave and Karst Studies*, v. 64, p. 108–116.
- RAILSBACK, L.B., LIANG, F., VIDAL ROMANÍ, J.R., GRANDAL-D'ANGLADE, A., VAQUEIRO RODRÍGUEZ, M., SANTOS FILDAGO, L., FERNANDEZ MOSQUERA, D., CHENG, H., AND EDWARDS, R.L., 2011, Petrographic and isotopic evidence for Holocene long-term climate change and shorter-term environmental shifts from a stalagmite from the Serra do Courel of northwestern Spain, and implications for climatic history across Europe and the Mediterranean: *Palaeogeography, Palaeoclimatology, Palaeoecology*, v. 305, p. 172–184.
- RAILSBACK, L.B., AKERS, P.D., WANG, L., HOLDRIDGE, G.A., AND VOARINTSOA, N.Y., 2013, Layer-bounding surfaces in stalagmites as keys to better paleoclimatological histories and chronologies: *International Journal of Speleology*, v. 42, p. 167–180.
- RAMAN, C.V., AND KRISHNAN, K.S., 1928, A new type of secondary radiation: *Nature*, v. 121, p. 501–502.
- REID, R.P., AND MACINTYRE, I.G., 1998, Carbonate recrystallization in shallow marine environments: a widespread diagenetic process forming micritized grains: *Journal of Sedimentary Research*, v. 68, p. 928–946.
- REPELLIN, P., 1977, Contribution à l'étude pétrologique d'un récif corallien: le sondage "Colette," atoll de Mururoa (Polynésie française): *Cahiers du Pacifique*, v. 20, p. 1–209.
- ROWLING, J., 2004, Studies on aragonite and its occurrence in caves including New South Wales caves: *Royal Society of New South Wales, Journal & Proceedings*, v. 137, p. 23–149.
- SANDBERG, P.A., 1984, Recognition criteria of calcitized skeletal and non-skeletal aragonites: *Palaeontographica Americana*, v. 54, p. 272–281.
- SARBU, S.M., AND LASCU, C., 1997, Condensation corrosion in Movile Cave, Romania: *Journal of Cave and Karst Studies*, v. 59, p. 99–102.
- SCHNEIDERMAN, N., AND HARRIS, P.M., 1985, Carbonate Cements: *SEPM, Special Publication* 36, 379 p.
- SELF, C.A., AND HILL, C.A., 2003, How speleothems grow: an introduction to the ontogeny of cave minerals: *Journal of Cave and Karst Studies*, v. 65, p. 130–151.
- SOUBIÉS, F., SEIDEL, A., MANGIN, A., GENTY, D., RONCHAIL, J., PLAGNES, V., HIROOKA, S., AND SANTOS, R., 2005, A fifty-year climatic signal in three stalagmite records from Mato Grosso, Brazil: *Quaternary International*, v. 135, p. 115–129.
- SUNAGAWA, I., 2005, *Crystals: Growth, Morphology and Perfection*: Cambridge, U.K., Cambridge University Press, 295 p.
- TAN, M., BAKER, A., GENTY, D., SMITH C., ESPER, J., AND CAI, B., 2006, Applications of stalagmite laminae to paleoclimate reconstructions: comparison with dendrochronology/climatology: *Quaternary Science Reviews*, v. 25, p. 2103–2117.
- TARHULE-LIPS, R., AND FORD, D.C., 1998, Condensation corrosion in caves on Cayman Brac and Isla de Mona: *Journal of Cave and Karst Studies*, v. 60, p. 84–95.
- THRILLKILL, J., 1968, Dolomite cave deposits from Carlsbad Caverns: *Journal of Sedimentary Petrology*, v. 38, p. 141–145.
- WASSENBERG, J.A., IMMENHAUSER, A., RICHTER, D.K., JOCHUM, K.P., FIETZKE, J., DEININGER, M., GOOS, M., SCHOLZ, D., AND SABAOUI, A., 2012, Climate and cave control on Pleistocene/Holocene calcite-to-aragonite transitions in speleothems from Morocco: Elemental and isotopic evidence: *Geochimica et Cosmochimica Acta*, v. 92, p. 23–47.

Received 19 July 2013; accepted 14 November 2013.